

# An attempt at estimating Paris area CO<sub>2</sub> emissions from atmospheric concentration measurements

F.M. Bréon<sup>1</sup>, G. Broquet<sup>1</sup>, V. Puygrenier<sup>1</sup>, F. Chevallier<sup>1</sup>, I. Xueref-Remy<sup>1</sup>, M. Ramonet<sup>1</sup>, E. Dieudonné<sup>1</sup>, M. Lopez<sup>1</sup>, M. Schmidt<sup>1</sup>, O. Perrussel<sup>2</sup>, P. Ciais<sup>1</sup>

[1]: {Laboratoire des Sciences du Climat et de l'Environnement, UMR CEA-CNRS-UVSQ, Gif sur Yvette, France}

[2]: {AirParif, 7 rue Crillon, Paris, France}

Correspondance to : F.M. Bréon, (breon@lsce.ipsl.fr)

## Abstract

Atmospheric concentration measurements are used to adjust the daily to monthly budget of fossil fuel CO<sub>2</sub> emissions of the Paris urban area from the prior estimates established by the Airparif local air quality agency. Five atmospheric monitoring sites are available, including one at the top of the Eiffel tower. The atmospheric inversion is based on a Bayesian approach, and relies on an atmospheric transport model with a spatial resolution of 2 km with boundary conditions from a global coarse grid transport model. The inversion adjusts a prior knowledge about the anthropogenic and biogenic CO<sub>2</sub> fluxes from the Airparif inventory and an ecosystem model, respectively, with corrections at a temporal resolution of 6 hours, while keeping the spatial distribution from the emission inventory. These corrections are based on assumptions regarding the temporal autocorrelation of prior emissions uncertainties within the daily cycle, and from day to day.

The comparison of the measurements against the atmospheric transport simulation driven by the a-priori CO<sub>2</sub> surface fluxes show significant differences upwind of the Paris urban area, which suggests a large and uncertain contribution from distant sources and sinks to the CO<sub>2</sub> concentration variability. This contribution advocates the inversion should aim at minimizing model-data misfits in upwind-downwind gradients rather than misfits in mole fraction at individual sites. Another conclusion of the direct model-measurement comparison is that the CO<sub>2</sub> variability at the top of the Eiffel tower is large and poorly represented by the model for

1 most wind speed and directions. The model inability to reproduce the CO<sub>2</sub> variability at the  
2 heart of the city makes such measurement ill-suited for the inversion. This and the need for  
3 constraining the budgets for the whole city suggests to assimilating upwind-downwind mole  
4 fraction gradient between sites at the edge of the urban area only.

5 The inversion significantly improves the agreement between measured and modelled  
6 concentrations gradients. Realistic emissions are retrieved for two 30-day periods and suggest  
7 a significant overestimate by the AirParif inventory. Similar inversions over longer periods  
8 are necessary for a proper evaluation of the optimized CO<sub>2</sub> emissions against independent  
9 data.

## 11 **1. Introduction**

12 Although the total CO<sub>2</sub> emissions of developed countries may be well constrained from the  
13 total consumption of fossil fuel, its spatial and temporal distribution are not known with the  
14 same level of accuracy. In so-called bottom-up emission estimates, CO<sub>2</sub> emission is  
15 calculated as a combination of geo-referenced activity proxies (e.g. road traffic data, or  
16 number and type of buildings that relate to residential emissions, (Gurney et al., 2012))  
17 multiplied by emission factors, accounting for the disaggregation of national annual budgets  
18 when dealing with regional or city inventories. The accuracy of the bottom-up inventories is  
19 seldom assessed and mostly relies on the difference between various estimates and on expert  
20 knowledge.

21 Due to the high population density associated with ground transportation, residence and  
22 industry, anthropogenic CO<sub>2</sub> emissions are large within cities (Pataki et al., 2006). The  
23 emitted CO<sub>2</sub> is transported in the atmosphere and results in elevated CO<sub>2</sub> concentration above  
24 and downwind of cities. There is therefore a potential to estimate the net CO<sub>2</sub> flux of a city  
25 from a few atmospheric concentration measurements located within or in the vicinity of the  
26 city (McKain et al., 2012). Over a very dense urban area, the net CO<sub>2</sub> flux is dominated by  
27 fossil fuel emissions, but over less dense urban structures, the net ecosystem exchange (NEE)  
28 becomes significant and can partly offset fossil CO<sub>2</sub> emissions during the growing season  
29 (Nordbo et al., 2012). Top-down net CO<sub>2</sub> flux estimates, constrained by independent  
30 atmospheric measurements, could come in complement to, or for the assessment of, current  
31 estimates that rely on bottom-up inventories.

1 The technique of estimating surface CO<sub>2</sub> fluxes from atmospheric composition measurements  
2 -and potentially from prior information- is relatively mature. It has been used for many years  
3 to estimate the biogenic fluxes at the global (Gurney et al., 2002;Chevallier et al., 2010),  
4 continental (Broquet et al., 2013;Peylin et al., 2005) and regional (Lauvaux et al.,  
5 2009;Lauvaux et al., 2012) scales. However, because of uncertainties in the atmospheric  
6 transport, insufficient measurement sampling, and inconsistencies between the mathematical  
7 framework hypothesis of most inversions (e.g. no biases, Gaussian distribution of errors,  
8 uncorrelated observation errors) and the reality, the results are not always consistent, in  
9 particular at the regional scale, as shown for instance through the recent comparison of global  
10 and continental-scale biogenic flux estimates by several global inversions (Peylin et al., 2013).

11 Estimating the net CO<sub>2</sub> flux of a city amplifies using similar mathematical and modelling  
12 tools amplifies the difficulties inherent to the atmospheric inversion. The spatial  
13 heterogeneity of the source and the possibility of having very high emissions locally (e.g. a  
14 power plant) make the structure of the prior error statistics complex and the concentration  
15 plume highly variable. Relating mole fractions to city sources further requires accurate  
16 atmospheric transport model at fine scale. Atmospheric transport in urban areas is influenced  
17 by specific meteorological processes such as higher roughness of urban canopies (Zhao et al.  
18 2014) and urban heat island effects (Nehrkorn et al., 2013). For instance, (Pal et al., 2012)  
19 reported significantly thicker boundary layer over the Paris city than in the surrounding rural  
20 area during a four day campaign that took place in March 2011, which was interpreted as a  
21 consequence of the urban heat island effect. Another difficulty, shared with the inversion of  
22 biogenic fluxes, lays in the temporal variability of the fossil fuel emissions, which have a  
23 strong daily cycle but also day-to-day variability resulting from, for instance, temperature  
24 changes (through heating) or activity (e.g. traffic) variability. Last, measurements in and  
25 around a target city collect CO<sub>2</sub> molecules of various origins that must be separated into city  
26 sources and remote sources and sinks through the inversion.

27 This challenge has been addressed recently by several research projects, e.g. INFLUX  
28 ([sites.psu.edu/influx](http://sites.psu.edu/influx), (Shepson et al., 2011)) over Indianapolis city or Megacities  
29 (<http://megacities.jpl.nasa.gov>; (Duren and Miller, 2012)) over Los Angeles, which have set-  
30 up a network of surface, tower and airborne measurements of the atmospheric CO<sub>2</sub> mole  
31 fractions. Satellite data may also provide valuable information as shown by (Kort et al.,  
32 2012). The results from the on-going urban CO<sub>2</sub> measurement project at Salt Lake City

1 indicated that monthly emission relative changes of 15% could be detected at the 95%  
2 confidence level with the current monitoring system (McKain et al., 2012) even though this  
3 study concluded on the inability to derive absolute estimates for a given month.

4 The CO<sub>2</sub>-MegaParis project has a similar objective for the Paris area. This is a potentially  
5 favourable case as the city is very dense and the emissions intense over a limited surface, with  
6 a fairly flat topography in the surroundings, which makes the atmospheric transport modelling  
7 easier. A pilot campaign early 2010 was conducted in the framework of the MEGAPOLI  
8 project. Measurements of the mole fraction of CO<sub>2</sub> and its isotopes have been used to  
9 estimate the relative contribution of fossil and biogenic emissions in the concentration  
10 gradients (Lopez et al., 2013). The main campaign started in August 2010 with the  
11 installation of three CO<sub>2</sub> and CO monitoring stations within the city and its surrounding that  
12 provided near-continuous measurements until July 2011. These three stations complement  
13 two stations of the ICOS France network located in the Paris region outside the city that have  
14 been operational for several years. (Lac et al., 2013) made a first analysis of the  
15 measurements and a comparison against atmospheric modelling using the Meso-NH  
16 mesoscale transport model, combined with a surface scheme that accounts for the urban  
17 environment, for a period of 5 days in March 2011. They demonstrated the ability of the  
18 modelling framework to reproduce several features of the mixing layer height, as reported in  
19 (Pal et al., 2012), and of the mole fraction daily cycle.

20 Large efforts have been made by AirParif, the air quality agency for the Paris area, to generate  
21 an inventory of the Paris area emissions, for various pollutants and for CO<sub>2</sub> as well. The  
22 AirParif emission inventory, detailed in section 2.2, provides an hourly description of the CO<sub>2</sub>  
23 emissions at  $\approx 1$  km resolution for representative weekdays and months. We use this  
24 inventory as an input to the atmospheric transport simulations and compare the results to the  
25 atmospheric concentration measurements from the five sites. We then attempt a correction of  
26 the inventory based on the differences between the observed and modelled mole fractions.  
27 With only 5 stations in the vicinity of the city, there is likely not enough information to  
28 constrain the spatial distribution of the emissions. We therefore only rescale the emissions,  
29 relying on the spatial distribution provided by the Airparif inventory. For the inversion, NEE  
30 and fossil fuel emissions are optimized separately. We focus on two 30-day periods in the fall  
31 of 2010. This choice is driven by the expectation of rather small biogenic fluxes during this  
32 time period, which makes easier the interpretation of the measurements in terms of

anthropogenic fluxes. Our objective is to assess whether a reliable estimate of the emissions at the daily to monthly time scales can be derived from the combination of atmospheric measurements, available inventories and information on the atmospheric transport. A forthcoming paper will apply the methodology to a full year of observations and analyse the result for the spring and summer periods, when CO<sub>2</sub> uptake by NEE can partially offset fossil fuel emissions (Pataki et al., 2007). In the following, section 2 analyses the time series of measured and modelled CO<sub>2</sub> mole fractions; section 3 describes the methodology to correct the inventory based on the measurement-model mismatches. The results are shown in section 4 while section 5 discusses the results and concludes.

## **2. Measurements and direct simulations**

### **2.1. CO<sub>2</sub> concentration measurements**

In this paper, we use CO<sub>2</sub> mole fraction measurements that have been acquired continuously in the framework of the CO<sub>2</sub>-Megaparis and ICOS-France projects. Three stations have been equipped with high precision CO<sub>2</sub>/CO analysers (Picarro G1302) specifically for the project objectives. One is located in the heart of Paris, at the summit of the Eiffel tower, 300 m above the surface. Two are located in the North and North-East of the Paris area in a mixed urban-rural environment. They are complemented by two ICOS-France stations that were operational before the start of the project. One is located in the South-West, about 20 km from the centre of Paris, while the other is a tall tower located further south by about 100 km. Both use gas chromatograph analysers (Agilent HP6890). The location of the stations are given in Table 1 and shown in Figure 1. They are very roughly located along a NE-SW direction, which defines the dominant wind directions, thus favourable for the monitoring of the CO<sub>2</sub> increase due to the emissions of the Paris area, with a station at the edge of the urban area in both directions. The measurements are quality-controlled and binned at a temporal resolution of 1 hour. They have been regularly calibrated against the WMO mole fraction scale (Zhao and Tans, 2006) so that measurement accuracy to the WMO-X2007 scale is estimated to be better than 0.38 ppm. The instrumental reproducibility is better than 0.17 ppm on the 5 minute average measurements available from the CO<sub>2</sub>-Megaparis stations, and the temporal averaging to the hourly-mean values used in this paper leads to precision much better than the accuracy (Zhao and Tans, 2006).

## 2.2. Atmospheric transport modelling

Atmospheric transport modelling provides the link between the surface fluxes and the atmospheric mole fractions. Here, we use the Chimere transport model (Menut et al., 2013) with a resolution of 2 km around the Paris city, and 10 km for the surrounding of the modelling domain (see Figure 1). There are 118x118 pixels in the modelling grid that covers an area of approximately 500x500 km<sup>2</sup>. There are 19 layers on the vertical, from the surface to 500 hPa. The Chimere transport model is driven by ECMWF-analysed meteorology at 15 km resolution. There is no urban scheme in the atmospheric modelling that is used here, which may be seen as a significant limitation to our inversion set-up. However, we conducted forward simulation comparisons between our modelling and that used in (Lac et al., 2013), which includes specific surface parameterization to account for the urban area, and we did not find significant differences on the simulated CO<sub>2</sub> mole fractions.

The model simulates the mole fractions that are driven by the surface fluxes and the boundary conditions. The surface fluxes that are accounted for in the simulations are the sum of

- Anthropogenic fossil fuel CO<sub>2</sub> emissions within the Île-de-France region, from the AirParif inventory, as described in section 2.3 and shown in Figure 2. Île-de-France is the administrative region spreading typically within 60 km around the Paris city, the boundaries of which are shown in Figure 1.
- Anthropogenic fossil fuel CO<sub>2</sub> emissions outside the Île-de-France region, according to the Edgar database [Edgar, 2011] available at 10 km resolution. These are only annual mean fluxes, and there is no description of the diurnal or seasonal cycle in this inventory.
- Biogenic fluxes from the C-TESSEL land surface model, as described in section 2.4.

The CO<sub>2</sub> boundary conditions prescribed at the lateral and top edges of the simulation domain, and transported inside the domain by Chimere, are obtained from the Monitoring Atmospheric Composition and Climate (MACC) global inversion, v10.2) (<http://www.copernicus-atmosphere.eu/>). In this simulation, the global distribution of surface CO<sub>2</sub> fluxes has been optimized to fit the mole fractions measured at a number of stations distributed over the world, given their assigned uncertainty and prior information of the surface fluxes. Given the relatively coarse spatial resolution of the transport model used in

the MACC inversion, CO<sub>2</sub> boundary conditions here are temporally and spatially very smooth and have little impact on the spatial gradients simulated within the domain area.

### 2.3. AirParif Inventory

The AirParif air quality agency (<http://www.airparif.asso.fr/en/index/index>) has developed an inventory of emissions (for greenhouse gases such as CO<sub>2</sub> but also for air pollutants) at 1 km spatial resolution and hourly time step for the Île-de-France region. The emissions are quantified by activity sectors. The improvement of methodologies and emission factors lead to frequent updates of the emission estimates.

Nearly eighty different source types are included in the inventory with three main classes: point sources, linear and diffuse sources. Point sources correspond to large industries, power plants, and waste burning; linear sources are related to transportation, while diffuse sources are mostly associated to the residential and commercial sectors. The road traffic emission estimates use a traffic model and vehicles counting devices that report the number of vehicles and their average speed over almost 40 000 km portions of roadways. Large industries are requested to report their CO<sub>2</sub> emissions and these are used in the inventory. For smaller industrial sources that are not required to report their emissions, a disaggregation of the regional fuel consumption is made based on the number of employees, leading to larger uncertainties. We have used the latest available version of the inventory, corresponding to year 2008, which has been developed for 5 typical months (January, April, July, August, and October) and three typical days (weekday, Saturday and Sunday) to account for the seasonal and weekly cycle of the emissions. Therefore this inventory estimates typical emissions but does not attempt to reproduce the daily variations resulting from specific meteorological conditions, or specific events such as public holidays.

Figure 2 shows an example of the spatial distribution of the total emissions for a weekday in October. Typical values are a few hundred gCO<sub>2</sub> m<sup>-2</sup> day<sup>-1</sup> within the city and a few tens gCO<sub>2</sub> m<sup>-2</sup> day<sup>-1</sup> in the suburbs. The main roads are clearly shown with flux enhancements of a few tens gCO<sub>2</sub> m<sup>-2</sup> day<sup>-1</sup>, at the 1 km<sup>2</sup> resolution of the inventory. Further processing of this map shows that one third of the Île-de-France emissions are within 10 km of the Paris centre, and 61% are within 20 km.

There is a large temporal variation of emissions, as shown in Figure 3, mostly at the daily scale, but also at the weekly and seasonal scales. Most components show a large daily cycle with minimum emissions at night. During the day, the traffic related emissions show several

maxima, in the morning, midday, and late afternoon. The daily cycles of the other activities are less pronounced but nevertheless significant. Point sources have the smallest daily cycle amplitude due to the industrial temporal profile that is relatively flat. The Paris area has few point sources and they contribute to typically 20% of the total emissions. The seasonal cycle is most pronounced for the residential emissions related to heating and cooking. One notes that residential CO<sub>2</sub> emissions do not go to zero during the summer months, because energy is still consumed for cooking and for heating water in summer.

In the following, the AirParif inventory for year 2008 is used as a prior estimate of the fossil fuel emissions within the Île-de-France region, both for the direct transport simulations (section 2.5) and for the flux inversion (section 3). Note that the inventory of point source emissions provides injection heights that have been used in the source term of the simulations. The AirParif inventory is provided as a function of legal time, and we have accounted for the time shift between legal time and UTC time, including the impact of daylight saving. Note that, due to the longitude of Paris, UT time and solar times are very similar.

## **2.4. Biogenic Fluxes**

The Net Ecosystem Exchange fluxes used here are provided by the land surface component of the ECMWF forecasting system, C-TESSEL (Boussetta et al., 2013). They are extracted from the ECMWF operational archives at the highest available resolution, 15 km and 3 hours. These data are interpolated in space (2 to 10 km) and time (1 hour) to be consistent with our atmospheric transport model grid and temporal resolution.

Figure 4 shows the mean daily cycle of NEE for the Île-de-France area and for the 12 calendar months. There are large diurnal and seasonal NEE cycles. The flux is positive (emission) during the night and negative (uptake) during the day, even during the winter months, given the rather mild winter temperature prevailing over the Paris area. Nevertheless, the amplitude of the daily cycle of NEE is much larger in summer than it is in winter. The NEE values are of similar magnitude than the anthropogenic emissions with a strong anti-correlation on the daily cycle (negative NEE vs. large anthropogenic emissions during daytime; positive NEE and smaller anthropogenic emissions during the night). During the winter, NEE is relatively small and the anthropogenic emissions clearly dominate, but daytime NEE still offsets on average ~20% of the emissions, according to the C-TESSEL model simulations. During spring and summer, however, the daytime NEE uptake is larger in absolute value than the anthropogenic emissions as shown through a comparison of Figures 3 and 4.



As our main interest is the anthropogenic emissions, we chose to analyse a period when the biogenic flux is small, i.e. during fall and winter. The present paper focuses on two 30-day periods that start on October 21<sup>st</sup> and November 27<sup>th</sup> 2010. During these periods, the monthly mean hourly NEE fluxes are less than 3 ktCO<sub>2</sub> per hour over the Île-de-France area. NEE is then small, but not negligible, compared to anthropogenic emissions during the chosen inversion periods.

## **2.5. Direct CO<sub>2</sub> transport simulations**

Figure 5, together with Figure S-1 in the supplementary, shows the time series of the CO<sub>2</sub> mole fractions together with an indication of the modelled wind speed and direction to help the interpretation of the results. These time series are derived from observations and direct atmospheric modelling as described in section 2.2.

The Trainou (TRN) station (bottom row) is far from the Paris agglomeration. In addition, the measurement inlet is at 180 m from the surface. It shows a diurnal cycle amplitude that is much smaller than at the other sites. In addition, the modelled contribution from both anthropogenic and biogenic fluxes within the simulation domains is limited to a few ppm, as shown by the difference between the black and green curve. There are a few exceptions however, essentially when the wind blows from the North, i.e. from the Paris city direction, and transports fossil CO<sub>2</sub> from the urban area to the TRN rural site. The best examples are around Dec 8<sup>th</sup> and Dec 23<sup>rd</sup>. For these particular cases, the measurements at TRN are significantly larger than the model results. The underestimate by the model is not limited to these dates and there are significant discrepancies between the model and the measurements at this remote background site, in particular at the end of November and at the beginning of December.

The other sites are much closer to Paris and are then more affected by the fossil CO<sub>2</sub> emissions. At Gif-sur-Yvette (GIF) the largest mole fractions are observed when the wind is from the North-East, which is expected as the Paris city is in that direction. There is also an impact of the wind, as the largest mole fractions are measured in low wind speed conditions. During the Oct-Nov period (Figure S-1), the wind is mostly from the South and South-West, thus not from the city, and there is a relatively good agreement between the modelled and measured mole fractions. In December, the wind direction is more variable, the fossil CO<sub>2</sub> signal appears much larger, and there are very significant differences between the measurements and the model estimates.

Gonesse (GON) is located to the North of the city, while Montgé-en-Goële (MON) is further away to the North-East. The shorter distance to the main source may explain the larger signal at the former station. The only cases when the modelled anthropogenic contribution is small at GON (small difference between black and green curve) is when the wind is from the North. For other wind directions, the modelled signal is strong -more than 10 ppm- and there are large differences between the measurements and the modelling results. During December, the measurements are most often larger than the model estimates. A similar observation can be made at MON. Surprisingly, the measurements are significantly larger than the modelling results, even when the wind blows from the North or North-East, i.e. when the Paris agglomeration contribution is negligible (Dec 3<sup>rd</sup>, Dec 6-9, Dec 22-23). For these cases, the most likely explanation is an underestimate of modelled CO<sub>2</sub> from the boundary conditions or from emissions within the modelling domain outside of Île-de-France. Hereafter, we shall denote this contribution as that from “remote fluxes”. Note that this impact from remote fluxes shows a large increase of the mole fraction for the periods discussed above. We may then hypothesize that this increase is underestimated. The interpretation is that anthropogenic emissions from the Benelux area generate high concentrations that are underestimated in the boundary condition field that is used in our simulations.

The EIF site is at the top of the Eiffel tower, 300 m above the Paris city. The wind speed for this station is larger than for the other one, simply because it is higher in altitude. One expects atmospheric mixing between the surface emissions and the inlet, so that the measurements are representative of a larger area than e.g. MON and GON. Nevertheless there are some very significant differences between the modelled and the observed mole fractions at EIF. The differences may be huge, larger than 30 ppm, even during the afternoon, e.g. on Oct 24<sup>th</sup>, Nov 7<sup>th</sup>, Dec 3<sup>rd</sup>, Dec 12<sup>th</sup>. Clearly, our atmospheric modelling framework cannot properly represent the mole fraction time series at the EIF station, either because of strong local (sub grid cell) emissions, or because of atmospheric transport processes that are not properly represented, in particular concerning the vertical transport above the city. Further analysis of the model-measurement mismatch is shown in Figure S-3. The largest mismatches are preferentially observed during the morning and for low wind speeds, but are observed at all hours of the day and for all wind speed and directions which prevents from attributing these mismatches to a specific bias in the transport model or to a bias in the estimate of the emissions for a specific area.

The curves in Figure 5 and Figure S-1 show very large temporal variations of CO<sub>2</sub> within a day at all stations. Further analysis confirms that the largest variations are observed during the night, when the mixing layer is shallow. During the night and morning, the atmosphere is often very stable so that surface emissions accumulate within the lowest atmospheric layers, the thickness of which ranges from a few meters to tens of meters. The atmospheric mole fraction is then mostly sensitive to local fluxes and vertical mixing -an atmospheric process that is difficult to model- so that there is a large uncertainty about the modelled link between the emissions and the atmospheric mole fraction. The night-time and morning measurements are thus not appropriate for our flux inversion, as inverting them would be too sensitive to atmospheric transport biases. As a consequence, we focus on the concentration measurements acquired during the afternoon only, from noon to 4 p.m., when the mixing layer is usually well developed. The daily averages of these afternoon measured and modelled values are shown in Figure 5 as diamond symbols.

Figure 6 shows a scatter plot of the measured and modelled mole fraction at the five sites together with the statistics of their comparison. The scatter plots confirm the visual impression of Figure 5: There is a significant correlation between the measured and modelled mole fraction, which demonstrates the model skill. There are also significant discrepancies and a large bias, in particular at the EIF station. The smallest errors (both biases and standard deviations) are found at TRN that is the site the furthest from Paris.

## **2.6. Analyses and insight for the inverse modelling configuration**

Both the measurements and the modelling results show some impact of the Paris area anthropogenic emissions on the CO<sub>2</sub> mole fractions at the 5 sites analysed here. The mole fraction increases over the modelled large-scale value depends on the wind speed and direction and a typical order of magnitude is 10 ppm. As expected, the signal is smaller for the rural station of TRN, which is further away from the city than the other sites. Many of the features in the measured time series are well reproduced by the modelling framework, which gives some confidence in its usefulness to improve the emission estimates.

There are also some significant differences between the measured and modelled mole fractions that cannot be justified by inaccurate emission inventories in the Paris area. The most obvious such feature is the mole fraction underestimate at MON and GON in northerly wind conditions when these sites are little sensitive to the Île-de-France emissions. This feature strongly suggests that remote fluxes lead to mole fraction increases that have biases

1 with a typical magnitude that is similar to the impact of the Paris area emissions. On the other  
2 hand, as the impact from remote fluxes is large scale, one may expect that this impact is  
3 similar for monitoring stations upwind and downwind from the Paris urban area. The model-  
4 measurement error may then be strongly reduced when analysing the difference of mole  
5 fractions between two stations that are located upwind and downwind the Paris urban area,  
6 respectively. On the other hand, the mole fraction difference between such stations that are  
7 close to the Paris area should contain a clear signature of the emissions from this area, and a  
8 relatively weak signature from other fluxes. It then suggests the use of downwind-upwind  
9 gradients in the CO<sub>2</sub> mole fractions rather than the absolute value of CO<sub>2</sub> measurements in the  
10 inversion procedure.

11 The other significant feature in the comparison of the modelled and measured CO<sub>2</sub> mole  
12 fractions is much larger errors at the EIF site than at the other stations. These results illustrate  
13 the difficulty in modelling the CO<sub>2</sub> mole fraction within cities, even with a measurement inlet  
14 in altitude, well above the sources. Note that (McKain et al., 2012) also find very large (>30  
15 ppm) model-measurement mismatches within the urban area of Salt Lake City, even when  
16 using a high-resolution model. Similarly (Lac et al., 2013) finds large model-measurements  
17 differences at EIF despite the use of an urban parameterization in the modelling. The inability  
18 to properly model the CO<sub>2</sub> signal at EIF may have detrimental impact on the emission  
19 estimates derived from atmospheric inversion. Conversely, the forward simulations show that  
20 the TRN site is little sensitive to the Paris area emissions due to its location further away from  
21 the city than the other sites. Consequently, it cannot be used as a “downwind” site; in  
22 addition, GIF is better suited as an “upwind site” for southerly conditions as it is closer to the  
23 urban area and provides therefore a better information on the air composition as it enters the  
24 city. These features suggest not to use EIF and TRN and rather focus on MON, GON and  
25 GIF to estimate the Paris area emission from their measured mole fractions.

26 The main objective of the “gradient” inversion method is thus to focus on the monitoring  
27 stations that are at the edge of the urban area and to estimate the city scale emissions by  
28 removing most of the upwind signal from the measured and modelled concentrations. The  
29 upwind signal is driven by remote fluxes both from the boundary conditions and by fluxes  
30 within the model domain but outside the city whose estimates bear very large uncertainties.  
31 The inversion method also attempts to select the downwind measurements that are affected by  
32 the emissions from a large part of the city, in an attempt to minimize the impact of

aggregation errors. Ideally, we would select only the wind direction when one station lies directly downwind from another, with the Paris city in between. However, given the very limited network of stations surrounding Paris, we have to broaden significantly the range of acceptable wind directions.

Based on this analysis, the emission estimate procedure only uses the measurements from GON, MON and GIF and is based on the CO<sub>2</sub> mole fraction gradients between the upwind and downwind stations, a method which requires the selection of favourable wind conditions. The mathematical framework is described in the next section while the inversion results are presented in section 4.

### 3. Flux inversion

#### 3.1. Principles

We follow a linear Bayesian inversion approach with Gaussian error statistics to determine the optimal surface fluxes (anthropogenic emissions and biogenic fluxes) and their uncertainties from a prior estimate of the fluxes and their uncertainties and from the mole fraction measurements.

We call  $\mathbf{x}$  the state vector that gathers the scaling factors for the 6-hourly flux maps,  $\mathbf{x}_B$  its prior estimate,  $\mathbf{H}$  the matrix operator that relates state parameters and mole fraction gradients according to the atmospheric transport model,  $\mathbf{y}$  the observed mole fractions gradients,  $\mathbf{y}_F$  the simulated impact on these mole fraction gradients of the lateral boundary conditions and of the fluxes that are not accounted for in the state vector,  $\mathbf{B}$  the uncertainty covariance matrix of  $\mathbf{x}_B$ , and  $\mathbf{R}$  the error covariance matrix of  $\mathbf{y}$ . These components are detailed in the next section.

The optimal solution is given by (Tarantola, 2005):

$$\mathbf{x}_A = \mathbf{x}_B + (\mathbf{B}^{-1} + \mathbf{H}^T \mathbf{R}^{-1} \mathbf{H})^{-1} \mathbf{H}^T \mathbf{R}^{-1} (\mathbf{y} - \mathbf{y}_F - \mathbf{H} \mathbf{x}_B) \quad (1)$$

and its posterior error covariance matrix is

$$\mathbf{A} = (\mathbf{B}^{-1} + \mathbf{H}^T \mathbf{R}^{-1} \mathbf{H})^{-1} \quad (2)$$

Note that  $\mathbf{A}$  does not depend on the actual measurement values, but varies, among other factors, with their temporal and spatial sampling.

#### 3.2. State vector: $\mathbf{x}$

Both the anthropogenic and biogenic prior fluxes described in Section 2 show a large diurnal cycle that impacts the model simulations of CO<sub>2</sub>, and that is uncertain. It then appears useful

to invert this cycle together with the flux daily mean values. However, as discussed earlier, only CO<sub>2</sub> measurements during the early afternoon can reliably be used to estimate the fluxes and their information about the daily cycle is rather poor. We limit the number of independent periods to 4 corresponding to the local times between 0-6 h, 6-12 h, 12-18 h, and 18-24 h, respectively.

For the fossil fluxes, we use a scaling factor for each individual day in the state vector, which makes the number of corresponding variables amount to 30×4=120 for the 30-day period of the inversion. These scaling factors apply to the prior flux estimates derived from the AirParif inventory and are noted  $\lambda_{0-6}^i, \lambda_{6-12}^i, \lambda_{12-18}^i, \lambda_{18-24}^i$  with i between 1 and 30.

Similarly, we optimize scaling factors of the prior NEE flux from C-TESSEL. The simulation domain shown in Figure 1 is split into 3×3 large boxes, and we choose the same 6-hour periods than for the anthropogenic fluxes to optimize scaling factors of NEE. However, we do not attempt a daily retrieval of NEE, and considered a single scaling factor for optimizing monthly NEE each 6-hour window over a 30-day inversion period. The number of variables to optimize NEE is therefore 3×3×4=36. In the following, these NEE scaling factors are shown as  $\alpha_{0-6}^X, \alpha_{6-12}^X, \alpha_{12-18}^X, \alpha_{18-24}^X$  where X is one of the 9 large boxes. One of the 9 boxes covers the Île-de-France region while the other ones are in the surrounding. In the *Inversion results* sections, we analyse the inversion of NEE for the centre box (X=C) together with those for the anthropogenic emissions. The surrounding boxes provide some ability to the inversion system to control part of the errors from remote NEE, but one cannot expect to get reliable estimate of the NEE in these areas given the weak observational constraint on this remote NEE.

The state vector **x** for the linear inversion has therefore 120+36 = 156 variables that represent the scaling factors to the modelled fluxes. The prior value of each of these scaling factors in **x<sub>B</sub>** is 1.

### 3.3. Measurements gradients: **y**

**y** contains the measurements gradients that are used to constrain the flux inversion. As explained above, we only use hourly measurements that have been acquired during the afternoon from noon to 4 p.m. local time. In addition, the corresponding measurements need to have a sensitivity to local, unresolved, fluxes that is insignificant in comparison to that of larger scale fluxes. This condition is not met when the wind speed is low. We therefore use

for the inversion only the measurements filtered for wind speeds larger than a given threshold at both sites used to compute the gradient. The results presented in this study are obtained with a threshold of  $2 \text{ m s}^{-1}$ . The wind speed estimate used for such a selection is the one analysed by the ECMWF at the location, height, and time of the observation. This criterion retains about 70% of the potential measurements.

In Equation (1) the downwind-upwind differences in mole fraction measurements  $y$  are corrected for the contributions that are not accounted for in the state vector ( $y_F$ ).  $y_F$  are the modelled mole fraction accounting for the boundary conditions and anthropogenic fluxes outside Île-de-France (prescribed from the Edgar database). This contribution is shown as a blue line in Figure 5 and Figure S-1.

When the wind is from the South-West (upwind direction between  $160^\circ$  and  $260^\circ$ ), GIF is considered as upwind from the urban area, and the corresponding  $y$  elements are the differences between the mole fractions measured at either MON or GON and that measured at GIF. Similarly, when the wind is from the North-East (upwind direction between  $0$  and  $135^\circ$ ), MON is used as an upwind reference to the GIF or GON mole fraction measurements. For other wind directions, the measurements are not assimilated.

### 3.4. Prior flux uncertainties and error correlations: B

Although we invert the scaling factors of fossil  $\text{CO}_2$  emissions for each day and each 6-hour period, the uncertainties in these factors are correlated. We therefore attempt to assign correlations for the prior uncertainties based on several considerations: (i) the monthly budget for the AirParif inventory is generally stated to have an uncertainty of 20% which is used here; (ii) we assume small positive correlations between the different 6-hour windows; (iii) we assume stronger correlations from day to day for a given 6-hour window; (iv) the a priori uncertainty of individual 6-hour emission should have a typical order of 50%.

Based on these considerations, we set, rather arbitrarily, prior error correlations to 0.4 for two adjacent time periods (e.g. 12-18 and 18-24) and to 0.2 for non-adjacent time period (e.g. 6-12 and 18-24). For successive days, we use an exponential de-correlation with a characteristic time  $T_{cor}$ . The correlation between the prior uncertainties of the fossil  $\text{CO}_2$  emissions scaling factors is then the product of this exponential and the time-periods correlation. For instance, the correlation between  $\lambda_{0-6}^5$  and  $\lambda_{6-12}^9$  is  $0.4 \exp(-4/T_{cor})$ . The results shown in this paper have been mostly obtained with a temporal correlation  $T_{cor}$  of 7 days, but other values, from 1

to 30 days, have been also tested. We have verified that such a **B** matrix is positive-definite. The desegregation of the assumed 20% uncertainty for the monthly emission totals, based on these temporal correlations, results in a standard deviation of uncertainties for individual 6-hour period of 33% ( $T_{cor}=30$  days) to 50% ( $T_{cor}=7$  days).

For the biogenic flux scaling factors, we set a relative prior uncertainty (standard deviation) close to 0.70 with some variations according to the box size (the variance varies inversely to the surface of the box), based on the numbers derived at 0.5° resolution in (Broquet et al., 2011). We do not assign any spatial / temporal correlation between the various biogenic scaling factors, i.e. between the 9 boxes or the 4 time periods. Similarly, there is no correlation in **B** between the prior uncertainties on the biogenic and anthropogenic fluxes.

### 3.5. Operator matrix: **H**

The operator matrix **H** provides the link between the surface fluxes and the mole fraction measurements. It combines the spatio-temporal distributions of the fluxes, both for the AirParif inventory and the C-Tessel biogenic fluxes, that are assumed and not modified through the inversion, the atmospheric transport by the Chimere model, the sampling of the atmosphere at the instrument locations and the selection of gradients according to the criteria developed in section 3.3. Note that the AirParif inventory has a 1 hour temporal resolution. The direct simulation (**H x**) uses the description of the emissions at this temporal resolution. Each element of the state vector corresponds to a natural or anthropogenic surface flux for a larger time period. We use the atmospheric transport model to compute the impact to the mole fraction of each surface flux (156 in total) corresponding to an element of the control vector. The 4D mole fraction fields from each of these simulations are then sampled at the place and time of the atmospheric observations used to compute the downwind-upwind gradients corresponding to the observation vector. These simulated mole fraction gradients provides the elements of each column of the **H** matrix.

### 3.6. Observation error: **R**

The measurements provided by the instrument are precise, certainly better than 0.3 ppm. However, the observation error in **R** also includes any source of misfit between the model and the data that is not accounted for in the state vector such as the representation error, the impact of the error in the spatial distribution of the fluxes, and the atmospheric transport modelling error. These are difficult to assess (Broquet et al., 2013) although one expects significant values given the very heterogeneous urban environment that is discussed here.



Due to the complexity and misunderstanding of the processes underlying the observation error, that may lead to positive or negative correlations, we ignore observation error correlations in the construction of  $\mathbf{R}$ , which is thus diagonal.

We use two statistical diagnostics of the misfits in the observation space described by (Desroziers et al., 2005) to infer typical observation error variances: (i) the agreement between the sum of the uncertainty from the prior estimate of the control parameters and of the observation error with the RMS of the prior misfits to the assimilated data; and (ii) the agreement between the observation error with the mean of the product of prior and posterior misfits to the assimilated data. Based on this analysis, we set a 3 ppm observation error for the mole fraction gradients that are used for the inversion.

We can note that this value is significantly smaller than the model-measurement differences as shown in Figure 5. This is due to the fact that the observation errors related to uncertainties in the large scale impact of the remote fluxes are strongly correlated between the measurement sites at a given time. Therefore, they vanish when considering gradients in the model fractions rather than values at individual sites such as in Figure 5. This is further discussed in section 4.2.

## **4. Inversion results**

In the following, we present the result of the inversion described in the previous section. We first analyse the modelled mole fractions, prior and posterior, against the measurements. We then analyse the retrieved fluxes, both NEE and fossil fuel.

### **4.1. Mole fraction gradients**

Figure 7 and Figure S4 show the time series of the afternoon-mean mole fraction gradients. Some days are missing either because either station is unavailable or because the wind direction does not fulfil the selection criteria developed in section 3.3. The prior value is almost always positive, because the reference is chosen upwind the Paris agglomeration. There are a few exceptions, like on Dec 22<sup>nd</sup> at GON, MON being used at the upwind reference according to the wind direction. As GON is in the northern part of the Paris agglomeration, one expects a smaller signal than for southerly wind conditions. Further investigation demonstrated that this unexpected behaviour is linked to a large spatial gradient of the CO<sub>2</sub> concentration generated by anthropogenic emissions over the Benelux accounted for in the Edgar inventory and transported by the Chimere model ( $y_F$  in equation 1).

1 Interestingly, the observations confirm the sign and the order of magnitude of the gradient  
2 that is modelled with our setup that uses crude anthropogenic emissions outside Île-de-France.

3 Another negative gradient is observed at GIF-MON for northerly wind conditions on Dec 3<sup>rd</sup>.  
4 This is very unexpected and we could not find a valid explanation for this particular case.

5 In general, the observations are smaller than the prior, and the posterior is in between.  
6 Indeed, the inversion result leads to concentration gradient that are closer to the observations.  
7 As a result, some of the posterior gradients are negative (see end of the period at GIF in  
8 Figure 7).

9 Figure 8 and Figure S4 show scatter plots of measured versus modelled mole fractions  
10 gradients. The first row of the plots on each of these figures shows the modelled mole  
11 fractions from the domain boundaries and the fossil CO<sub>2</sub> emission outside Île-de-France  
12 (black lines in Figure 5,  $y_F$  in equation 1) against the measurement. This constitutes the  
13 modelled contribution to the mole fraction that is not optimized by the inversion. The values  
14 on the Y-axis show the modelled impact of the remote fluxes on the upwind-downwind mole  
15 fraction gradient. As expected, this impact is small compared to the measured gradient shown  
16 on the X-axis.

17 The second row shows simulated CO<sub>2</sub> induced by prior NEE and fossil CO<sub>2</sub> fluxes (i.e. those  
18 that are optimized through the inversion) against measured mole fractions corrected for the  
19 large scale values (i.e.  $y_F$ , shown on the Y-axis of the first row). Although there is a large  
20 spread, the correlation is significant, which shows that the transport model and the prior flux  
21 set up have altogether some ability to reproduce the observed CO<sub>2</sub> mole fraction variability.  
22 For the Oct-Nov period (in supplementary), the biases are large for all site gradients (2.1 to  
23 4.8 ppm) whereas, for the Nov-Dec period, they are even larger at GIF-MON (7.1 ppm) but  
24 rather small in comparison at both other sites. The standard deviation of the measurement-  
25 model difference varies with the sites and period, between 2.0 and 5.8 ppm. This is  
26 significantly smaller than the standard deviation for the mole fractions (Figures 6 and Figure  
27 S2) that vary between 3.6 and 6.6 ppm. These smaller values confirm the choice made of  
28 attempting an inversion based on the mole fraction gradient rather than the individual  
29 observations.

30 After the inversion, the agreement is significantly improved as shown in the third row. Note  
31 however that the standard deviation for the MON site (when GIF is used as a reference) is  
32 slightly degraded from the prior value of 2.0 ppm. After the inversion, the correlation

between optimized and observed CO<sub>2</sub> gradients for all three stations is larger than 0.90. For the other time period shown in the supplementary material (Figure S-5), the correlation statistics are not as good. However, this is due to a lower variability of the gradients, and the posterior standard deviations are 2.3, 2.7 and 2.3 ppm for the three sites, and are then similar as the values shown in Figure 7.

Overall, the statistics improve significantly between the prior and the posterior, and there is a good agreement between the measured and modelled mole fraction gradients. This raises confidence in our ability to model the impact of the Paris CO<sub>2</sub> emissions on the atmospheric concentrations for various wind conditions.

## **4.2. Daily flux estimates**

Figure 9 shows the daily anthropogenic fluxes inferred by the inversion procedure. Here, we have aggregated the 4 6-hour periods as well as their uncertainty, accounting for the error correlations between the periods. Although the inversion controls scaling factors, we show here the resulting fluxes expressed in MtCO<sub>2</sub> per day. There is a clear weekly cycle on the prior emissions that are smaller during the week-ends. One may also note a shift in prior emission between Oct 29<sup>th</sup> and Nov 1<sup>st</sup> that corresponds to a change of month and therefore the switch to a different dataset in the AirParif inventory. The Airparif inventory includes a profile for October. For November and December, Airparif recommends the use of the January emission profile.

The uncertainty reduction is significant for all the days of the two time periods and a typical order of magnitude is a factor of 2. The emission uncertainty is reduced even for days with no usable measurements, when the wind direction is not within any of the two ranges defined in section 3.3, due to the temporal correlation of the uncertainties and thus of the corrections applied to the prior (section 3.4). The deviations of the flux estimate from the prior follow the gradient observation deviation from the model (see Figure 7). These deviations are mostly negative, although they are positive for a few days during both time periods. For the Nov-Dec period, the posterior emission estimates are within the bounds of the prior uncertainty range. On the other hand, the posterior estimate is much lower than the prior flux during the second half of the Oct-Nov period (Figure 9, top). Interestingly this period (Nov 1<sup>st</sup> to Nov 20<sup>st</sup>, 2010) was very mild [Meteo France, 2010] which suggests that the heating sector emissions were well below the AirParif inventory values for that period. During this season, according to the AirParif inventory, the heating sector, commercial and residential, amounts

to more than 50% of the emission, so that the total emission is highly sensitive to temperature. Note that AirParif recommends the use of the January inventory for both November and December. As the temperatures are generally milder during October than January, one may expect that the inventory is larger than the true fluxes during October, which is then consistent with the negative correction to the fluxes during that period.

Figure 9 was generated using a 7 day correlation time for the emission uncertainties. We also tested similar inversions using different error correlation times ( $T_{cor}$ ) in the range of the synoptic to seasonal time scales that drives the emission variability to assess the result sensitivity to this parameter. With a 1 day error correlation time, rather than 7 days used in our standard configuration, there are days with little or no flux constrain by the observations, while there is no smoothing of the day-to-day variability correction, resulting in an even larger spread of the retrieved fluxes (not shown). At the other extreme, a 30-day correlation time leads to much smoother results. Most of the daily-optimized flux estimates remain within the prior uncertainty range.

### 4.3. Monthly budgets

Figure 10 shows the monthly mean flux estimates for the Île-de-France region for the various 6-hour periods. It shows the results of the inversion for the anthropogenic emissions, the NEE of the central box that covers Ile de France, as well as the total. Note that the total estimate is necessarily the sum of the biogenic and anthropogenic fluxes. Conversely, the uncertainty range of the total is not a simple sum as it accounts for the correlations between NEE and fossil CO<sub>2</sub> emission errors in the **A** matrix linked to the difficulty in distinguishing NEE and fossil fluxes from the measurements.

The inversion has little impact on the fluxes for the 0-6h and 18-24h periods. On the other hand, the impact is strong for the 6-12h and 12-18h periods. This is because we only use afternoon observations that are sensitive to the emissions from the morning and afternoon periods only. The assigned correlations in the setup of the **B** matrix transport some constrain to the other time windows. Although the inversion based on the mole fraction gradients uses few independent observation, because of the additional data selection based on the wind direction, the impact on the flux estimates is significant.

Figure 10 shows that the uncertainty reduction is much larger for the fossil fuel than for the NEE. This is the result of the inversion based on the gradient downwind-upwind from the city which are mostly sensitive to the fluxes in between. The contribution from the NEE to

the measurement is then small. Nevertheless, the correlations on the anthropogenic and NEE uncertainties are small ( $\pm 0.15$  or less). These numbers indicate that the observation sampling provides significant information to distinguish NEE from fossil CO<sub>2</sub> fluxes in the inversion. Although a given measurement cannot trace the origin of the mole fraction excess, the assigned biogenic and anthropogenic flux errors have different spatial and temporal patterns which are exploited by the inversion system to attribute the mole fraction signal to specific sectors. However, this attribution relies on the a-priori spatial and temporal distribution of the fluxes that are affected by uncertainties. Thus, the theoretical ability of the system to disentangle natural and anthropogenic fluxes may not be realized in practice.

## 5. Discussion and Conclusions

This paper is a first attempt at estimating the Paris area emissions from measurements of atmospheric CO<sub>2</sub> mole fractions and prior flux knowledge. There is obviously room for improvement in several aspects of the inversion system: the number and spatial distribution of the monitoring stations, the atmospheric transport model including the use of an urban scheme, the modelling of concentration at the simulation domain boundaries, the definition of the emissions outside Île-de-France, the definition of the control vector, etc. However, first conclusions of broad implications beyond this first attempt can be drawn, that should guide further inverse modelling developments for Paris and other cities.

The analysis of the CO<sub>2</sub> time series shows significant differences between the measured and modelled mole fractions upwind the Paris city. These differences indicate that the simulated mole fraction at the domain boundaries may be off by several ppm. The errors in this simulation are of similar magnitude as the signal from the Paris area emissions. Although the number of cases is limited, it seems that the boundary concentrations are significantly underestimated when the wind is from the North or North-East (Benelux). These uncertainties on the domain boundaries generate large scale errors in the modelled mole fraction and suggest applying the inversion not on the measurements themselves, but rather on upwind-downwind gradients as was done in this paper. Indeed, the measurement-model agreement is much better for the gradients than it is for the direct values. It confirms that the large-scale pattern of CO<sub>2</sub> mole fraction, which is not related to the Île-de-France fluxes, is not properly modelled. The information provided by our five-site network does not allow optimizing the structure of the CO<sub>2</sub> boundary conditions, which is directly prescribed by a

1 coarse scale global inversion. Exploiting the distant sites currently operational in Europe  
2 would unlikely improve this situation. In this context, the inversion based upon gradients as  
3 presented in section 4 appears necessary. It relies on the assumption that, due to atmospheric  
4 diffusion, the signature of remote fluxes upwind the city is sufficiently homogeneous in  
5 space, horizontally and vertically, and time over the path through the city from upwind to  
6 downwind sites both located within the afternoon PBL. As a consequence, the main part of  
7 such a large-scale signal is removed through the differences between two sites. The validity  
8 of this hypothesis is confirmed by the much better agreement between measured and  
9 modelled mole fractions as shown through the comparison of Figure 6 and Figure 8. Both  
10 measurements and atmospheric transport simulations indicate, however, that the CO<sub>2</sub> mole  
11 fraction signal generated by distant sources outside the Chimere model domain has some  
12 spatial structures (see e.g. the variability of modelled values in Figure 8-top) which needs to  
13 be accounted for.

14 The drawback of using the gradient-based inversion method is a reduction in the number of  
15 observations, in particular with the current monitoring network that only samples a fraction of  
16 possible wind directions. Nevertheless, although the number of observations is very much  
17 reduced, our inversion system based on the gradient reports significant uncertainty reductions.  
18 It must also be noted that we assumed a 7-day error correlation time for the anthropogenic  
19 emissions, so that our system shows flux uncertainty reductions, even on days with no valid  
20 observation as the flux is constrained by observation of the previous or following days.

21 The setting of temporal error correlation on prior fluxes is therefore essential for the  
22 inversion. Although the results in this paper are mostly derived with a 7-day correlation  
23 length, this is a somewhat arbitrary choice, and the results are significantly affected when  
24 using different values. In particular, a much shorter value (1 day) leads to very large  
25 variations in the posterior daily emissions. Further work should be devoted to the assignment  
26 of objective correlation lengths based on the processes that lead to emission uncertainties.  
27 Climatic conditions in general, and more specifically temperature during the cold season,  
28 influence the emission with a time scale that is consistent with synoptic events, i.e. close to a  
29 week; the impact of specific events such as holidays, commemorations or strikes have a much  
30 shorter time scale, while inventory biases linked to e.g. the emission factors have an impact  
31 on the fluxes on time scales of months or even larger.

1 Our analysis also indicates model-measurement discrepancies at the EIF site that are much  
2 larger than at other sites. On the one hand, this is somewhat surprising as measurement inlet  
3 in altitude should insure a larger spatial representativeness than at the surface sites and less  
4 sensitivity to local, poorly represented, emissions. Usually, tall tower-based measurements  
5 are preferred to those at the surface for the estimate of biogenic fluxes. On the other hand,  
6 EIF is located close to the centre of the Paris city and is therefore affected by stronger local  
7 emissions than the other sites used in this paper. City fluxes are highly heterogeneous while  
8 the model used in this paper has a 2 km spatial resolution, does not include information on the  
9 3D structure of the urban canopy, and uses limited information on the CO<sub>2</sub> source injection  
10 heights. Such model may then be insufficient to properly account for atmospheric processes  
11 that link the local surface fluxes to the concentrations at the top of the Eiffel tower. Previous  
12 results obtained at MeteoFrance by (Lac et al., 2013) using a high (2 km) resolution  
13 meteorological model that includes urban parameterizations, and validated against local  
14 meteorological measurements, also show high model-data misfits at EIF, similar to those  
15 found in the present paper. (McKain et al., 2012) also show a poor skill at representing the  
16 mole fraction at urban sites, so that the information content of the measurements is not  
17 applied for an estimate of the absolute emissions, but rather for a on long term relative  
18 change. These findings can be related to our difficulties for modelling urban CO<sub>2</sub> at EIF using  
19 a 2 km resolution transport model are typical of the current generation of models. The use of  
20 urban sites such as EIF for atmospheric inversion will likely necessitate long term research by  
21 the inverse modelling and transport modelling communities.

22  
23 At present, our mesoscale atmospheric transport model cannot reconcile the measurements at  
24 the top of the tower with those at the surface in the vicinity of the city, given our set of  
25 surface fluxes and inversion settings. This cast doubts on the quality of the modelling at the  
26 other sites. Indeed, if the atmospheric transport model does not properly simulate the  
27 atmospheric vertical transport between the surface and an inlet at 300 m in altitude, it likely  
28 misrepresents the link between surface fluxes and atmospheric mole fractions. Conversely,  
29 the large modelling errors at EIF may be related to its urban location (and to the strong  
30 influence of local urban sources) and this would raise concerns regarding the ability to exploit  
31 urban measurements, and therefore to solve for the spatial distribution of the fluxes within the  
32 urban area.

1  
2 The largest differences between the measured and modelled concentrations occur for low  
3 wind speeds. For this reason, we have chosen a  $2 \text{ m s}^{-1}$  wind speed threshold below which the  
4 measurements are not used in the inversion. A larger threshold rejects further observations,  
5 and reduces the range of flux corrections through the inversion. The choice of the threshold is  
6 somewhat arbitrary and we have refrained from using a large one to clearly demonstrate the  
7 impact of a few situations with low wind-speed. There are several hypotheses for the poor  
8 modelling at low wind speed, including larger representativity errors of subgrid patterns, or  
9 larger errors in vertical mixing modelling. However, such issues are continuous and there is  
10 no indication that the modelling errors disappear between e.g.  $2$  and  $3 \text{ m s}^{-1}$ . Thus, further  
11 rejection of low wind-speed observations may hide the deficiencies in the atmospheric  
12 transport without improving the flux inversion.

13  
14 We also stress that our analysis is based on measurements during the late fall period. This is a  
15 favourable case for the inversion of fossil fuel  $\text{CO}_2$  emissions as there is less interference with  
16 the biogenic fluxes (Pataki et al., 2007). During spring and summer, the NEE is much larger  
17 (in absolute value) and also more uncertain. In fact, during May, the biogenic sink is likely  
18 larger than the anthropogenic emissions within Île-de-France as shown by Figure 3 and Figure  
19 S4. The gradient inversion method is designed to also minimize this interference of biogenic  
20 flux with the constraint on anthropogenic fluxes. Indeed, the theoretical posterior  
21 uncertainties indicate little correlations between the retrieved NEE and anthropogenic  
22 emissions. There is however vegetation within the urban area that may generate a significant  
23 sink during the growing season. A successful anthropogenic emission inversion would  
24 benefit from additional efforts for describing the biogenic fluxes and the use of additional  
25 tracers such as  $^{14}\text{C}$  to separate the signature of fossil fluxes and biogenic emissions. One  
26 future direction is thus to use a more realistic NEE model over the Paris area, that could be  
27 calibrated upon local eddy covariance observations (e.g. the method used in (Gerbig et al.,  
28 2003)) and satellite land cover and vegetation activity.

29  
30 The prior estimate of the Île-de-France  $\text{CO}_2$  emissions does not account for the human  
31 respiration. Yet, within dense urban areas, human respiration can be a significant fraction of  
32 the fossil fuel emissions (Ciais et al., 2007) (Widory and Javoy, 2003). Respiration by human



1 beings is a source of CO<sub>2</sub> of typically 1 kgCO<sub>2</sub> day<sup>-1</sup> (Prairie and Duarte, 2007) which,  
2 assuming a total population of 11.7 millions for the Île-de-France, leads to 4.2 MtCO<sub>2</sub> per  
3 year, or 8% of the AirParif fossil fuel inventory. Although small, this flux is far from  
4 negligible compared to fossil fuel emissions. While the CO<sub>2</sub> mole fraction measurements are  
5 sensitive to the human respiration flux, our control vector only accounts for the fossil fuel  
6 emissions and NEE fluxes. Although it does not have point sources, the spatial distribution of  
7 the human respiration is broadly similar to that of the fossil fuel emissions, so that the  
8 inversion will attribute the human respiration mole fraction signal to the fossil fuel rather than  
9 the NEE fluxes. We therefore expect an overestimate of the fossil fuel emission by typically  
10 8% in our inversion that neglects human respiration. A larger percentage may be expected in  
11 summer and a smaller in winter due to the seasonal cycle of the fossil fuel emissions that has  
12 a larger relative amplitude than that of the human respiration. Improvement of our inversion  
13 system should explicitly account for the human respiration, based on the spatial distribution of  
14 the population.

15  
16 One often stated objective of the top-down inversion of fossil fuel CO<sub>2</sub> emissions is to  
17 provide an independent verification of the bottom-up estimates, i.e. the inventories (Levin et  
18 al., 2011; McKain et al., 2012; Duren and Miller, 2012). However, information about the  
19 spatial and temporal distribution of the emissions has to be used for inverse modelling to limit  
20 aggregation errors on the overall budget. In our case, the number of monitoring stations is far  
21 too small to independently invert the spatial distribution of the emissions. We have been able  
22 to rely on the comprehensive distribution from AirParif. With a larger number of monitoring  
23 stations, it may be possible to estimate some information about the flux spatial distribution,  
24 but atmospheric transport is not a reversible process and some accurate information about the  
25 spatial distribution will likely be needed, so that the atmospheric inversion cannot be seen as  
26 independent from the inventories, but rather as a mean to verify or refine them. In addition,  
27 as long as the accuracy on the atmospheric transport makes does not allow using night-time or  
28 morning measurements, it will not be possible to monitor the daily cycle of the emissions.  
29 Thus, the computation of daily or monthly fluxes requires some robust information about the  
30 daily cycle that should rely on inventories. Thus, again, our top-down emission estimate is far  
31 from independent from the bottom-up inventory.

1 Although the inversion procedure provides a posterior uncertainty estimate, one should  
2 interpret this uncertainty with caution. Indeed, the mathematical framework used here relies  
3 on a number of hypotheses, some of which are crude approximations of the reality, such as  
4 the spatial and temporal correlations in the flux uncertainties or the unbiased atmospheric  
5 transport modelling. The impact of these assumptions has not been quantified. Although we  
6 have no “truth” to benchmark the inversion results, and there are not even enough  
7 measurement sites to perform ‘leave-one-out’ tests, one can perform some sanity checks on  
8 the results. One sanity check is the comparison of the measured and modelled mole fractions  
9 (Figure 8 and Figure S4). The analysis of these figures confirms the ability of our inversion  
10 to improve the measurement-model agreement. Nevertheless, we note that the posterior  
11 misfit ( $\approx 2.5$  ppm) is still a significant fraction of the signal that is analysed (10-20 ppm). The  
12 crucial question is whether the atmospheric modelling error is random or a bias and we have  
13 no element to answer that question. The other sanity check consists in analysing the validity  
14 of the retrieved daily fluxes (Figure 9). In this respect, the daily fluxes show day-to-day  
15 variations that are suspicious, although not refutable at this stage. A result that points in  
16 favour of the flux inversions shown here is the significant reduction from the prior during a  
17 period with temperatures above the seasonal normal, and the negative correction of the  
18 emissions during November from the prior value that is based on an inventory simulating  
19 January emissions. A single such event is certainly not sufficient to validate the inversion  
20 system, however. We shall apply the same inversion setup to more than a year of  
21 measurements and analyse the results with respect to the temperature anomaly or other short-  
22 term event that may have a significant influence on the Île-de-France CO<sub>2</sub> emissions. More  
23 measurement sites are needed to better evaluate the skill of the inversion. The deployment of  
24 a network of 5 sites around Paris within the framework of the CarboCount-City project will  
25 help in this direction. In addition, inlet at different altitudes will be installed on the Eiffel  
26 tower station for a better assessment of the CO<sub>2</sub> vertical distribution and transport within the  
27 urban area. These will be most useful for the longer-term objective of improving the  
28 atmospheric transport modelling within the city, which may allow the EIF measurements to  
29 be used by the inversion system.

## Acknowledgments

This study was conducted within the ANR CO2-Megaparis project and was made possible thanks to funding from the CarboCount and CarboCount-city projects that are co-funded by the Climate KIC program of the European Institute of Technology. Gregoire Broquet acknowledges funding and support from the Chaire industrielle BridGES, a joint research program between Thales Alenia Space, Veolia, Université de Versailles Saint Quentin en Yvelines, CEA and CNRS. We thank Lin Wu and Isabelle Pison for assistance as well as all the developers of the AirParif inventory.

## References

- Boussetta, S., Balsamo, G., Beljaars, A., Panareda, A. A., Calvet, J. C., Jacobs, C., van den Hurk, B., Viterbo, P., Lafont, S., Dutra, E., Jarlan, L., Balzarolo, M., Papale, D., and van der Werf, G.: Natural land carbon dioxide exchanges in the ECMWF integrated forecasting system: Implementation and offline validation, *J Geophys Res-Atmos*, 118, 5923-5946, Doi 10.1002/Jgrd.50488, 2013.
- Broquet, G., Chevallier, F., Rayner, P., Aulagnier, C., Pison, I., Ramonet, M., Schmidt, M., Vermeulen, A. T., and Ciais, P.: A European summertime CO2 biogenic flux inversion at mesoscale from continuous in situ mixing ratio measurements, *J Geophys Res-Atmos*, 116, Artn D23303, doi 10.1029/2011jd016202, 2011.
- Broquet, G., Chevallier, F., Breon, F. M., Kadyrov, N., Alemanno, M., Apadula, F., Hammer, S., Haszpra, L., Meinhardt, F., Morgui, J. A., Necki, J., Piacentino, S., Ramonet, M., Schmidt, M., Thompson, R. L., Vermeulen, A. T., Yver, C., and Ciais, P.: Regional inversion of CO2 ecosystem fluxes from atmospheric measurements: reliability of the uncertainty estimates, *Atmos Chem Phys*, 13, 9039-9056, Doi 10.5194/Acp-13-9039-2013, 2013.
- Chevallier, F., Ciais, P., Conway, T. J., Aalto, T., Anderson, B. E., Bousquet, P., Brunke, E. G., Ciattaglia, L., Esaki, Y., Frohlich, M., Gomez, A., Gomez-Pelaez, A. J., Haszpra, L., Krummel, P. B., Langenfelds, R. L., Leuenberger, M., Machida, T., Maignan, F., Matsueda, H., Morgui, J. A., Mukai, H., Nakazawa, T., Peylin, P., Ramonet, M., Rivier, L., Sawa, Y., Schmidt, M., Steele, L. P., Vay, S. A., Vermeulen, A. T., Wofsy, S., and Worthy, D.: CO2 surface fluxes at grid point scale estimated from a global 21 year reanalysis of atmospheric measurements, *J Geophys Res-Atmos*, 115, Artn D21307, doi 10.1029/2010jd013887, 2010.
- Ciais, P., Bousquet, P., Freibauer, A., and Naegler, T.: Horizontal displacement of carbon associated with agriculture and its impacts on atmospheric CO2, *Global Biogeochem Cy*, 21, Artn Gb2014, doi 10.1029/2006gb002741, 2007.
- Desroziers, G., Berre, L., Chapnik, B., and Poli, P.: Diagnosis of observation, background and analysis-error statistics in observation space, *Q J Roy Meteor Soc*, 131, 3385-3396, Doi 10.1256/Qj.05.108, 2005.
- Duren, R. M., and Miller, C. E.: COMMENTARY: Measuring the carbon emissions of megacities, *Nat Clim Change*, 2, 560-562, 2012.

1 Gerbig, C., Lin, J. C., Wofsy, S. C., Daube, B. C., Andrews, A. E., Stephens, B. B., Bakwin,  
2 P. S., and Grainger, C. A.: Toward constraining regional-scale fluxes of CO<sub>2</sub> with  
3 atmospheric observations over a continent: 1. Observed spatial variability from airborne  
4 platforms, *J Geophys Res-Atmos*, 108, Artn 4756, doi 10.1029/2002jd003018, 2003.

5 Gurney, K. R., Law, R. M., Denning, A. S., Rayner, P. J., Baker, D., Bousquet, P., Bruhwiler,  
6 L., Chen, Y. H., Ciais, P., Fan, S., Fung, I. Y., Gloor, M., Heimann, M., Higuchi, K., John, J.,  
7 Maki, T., Maksyutov, S., Masarie, K., Peylin, P., Prather, M., Pak, B. C., Randerson, J.,  
8 Sarmiento, J., Taguchi, S., Takahashi, T., and Yuen, C. W.: Towards robust regional  
9 estimates of CO<sub>2</sub> sources and sinks using atmospheric transport models, *Nature*, 415, 626-  
10 630, Doi 10.1038/415626a, 2002.

11 Gurney, K. R., Razlivanov, I., Song, Y., Zhou, Y. Y., Benes, B., and Abdul-Massih, M.:  
12 Quantification of Fossil Fuel CO<sub>2</sub> Emissions on the Building/Street Scale for a Large US  
13 City, *Environ Sci Technol*, 46, 12194-12202, Doi 10.1021/Es3011282, 2012.

14 Kort, E. A., Frankenberg, C., Miller, C. E., and Oda, T.: Space-based observations of  
15 megacity carbon dioxide, *Geophys Res Lett*, 39, Artn L17806, doi 10.1029/2012gl052738,  
16 2012.

17 Lac, C., Donnelly, R. P., Masson, V., Pal, S., Riette, S., Donier, S., Queguiner, S., Tanguy,  
18 G., Ammoura, L., and Xueref-Remy, I.: CO<sub>2</sub> dispersion modelling over Paris region within  
19 the CO<sub>2</sub>-MEGAPARIS project, *Atmos Chem Phys*, 13, 4941-4961, Doi 10.5194/Acp-13-  
20 4941-2013, 2013.

21 Lauvaux, T., Pannekoucke, O., Sarrat, C., Chevallier, F., Ciais, P., Noilhan, J., and Rayner, P.  
22 J.: Structure of the transport uncertainty in mesoscale inversions of CO<sub>2</sub> sources and sinks  
23 using ensemble model simulations, *Biogeosciences*, 6, 1089-1102, 2009.

24 Lauvaux, T., Schuh, A. E., Uliasz, M., Richardson, S., Miles, N., Andrews, A. E., Sweeney,  
25 C., Diaz, L. I., Martins, D., Shepson, P. B., and Davis, K. J.: Constraining the CO<sub>2</sub> budget of  
26 the corn belt: exploring uncertainties from the assumptions in a mesoscale inverse system,  
27 *Atmos Chem Phys*, 12, 337-354, Doi 10.5194/Acp-12-337-2012, 2012.

28 Levin, I., Hammer, S., Eichelmann, E., and Vogel, F. R.: Verification of greenhouse gas  
29 emission reductions: the prospect of atmospheric monitoring in polluted areas, *Philosophical*  
30 *transactions. Series A, Mathematical, physical, and engineering sciences*, 369, 1906-1924,  
31 10.1098/rsta.2010.0249, 2011.

32 Lopez, M., Schmidt, M., Delmotte, M., Colomb, A., Gros, V., Janssen, C., Lehman, S. J.,  
33 Mondelain, D., Perrussel, O., Ramonet, M., Xueref-Remy, I., and Bousquet, P.: CO, NO<sub>x</sub> and  
34 (CO<sub>2</sub>)-C-13 as tracers for fossil fuel CO<sub>2</sub>: results from a pilot study in Paris during winter  
35 2010, *Atmos Chem Phys*, 13, 7343-7358, Doi 10.5194/Acp-13-7343-2013, 2013.

36 McKain, K., Wofsy, S. C., Nehrkorn, T., Eluszkiewicz, J., Ehleringer, J. R., and Stephens, B.  
37 B.: Assessment of ground-based atmospheric observations for verification of greenhouse gas  
38 emissions from an urban region, *P Natl Acad Sci USA*, 109, 8423-8428, Doi  
39 10.1073/Pnas.1116645109, 2012.

40 Menut, L., Bessagnet, B., Khvorostyanov, D., Beekmann, M., Blond, N., Colette, A., Coll, I.,  
41 Curci, G., Foret, G., Hodzic, A., Mailler, S., Meleux, F., Monge, J. L., Pison, I., Siour, G.,  
42 Turquety, S., Valari, M., Vautard, R., and Vivanco, M. G.: CHIMERE 2013: a model for  
43 regional atmospheric composition modelling, *Geosci Model Dev*, 6, 981-1028, Doi  
44 10.5194/Gmd-6-981-2013, 2013.

- 1 Nehr Korn, T., Henderson, J., Leidner, M., Mountain, M., Eluszkiewicz, J., McKain, K., and  
2 Wofsy, S.: WRF Simulations of the Urban Circulation in the Salt Lake City Area for CO<sub>2</sub>  
3 Modeling, *J Appl Meteorol Clim*, 52, 323-340, Doi 10.1175/Jamc-D-12-061.1, 2013.
- 4 Nordbo, A., Jarvi, L., Haapanala, S., Wood, C. R., and Vesala, T.: Fraction of natural area as  
5 main predictor of net CO<sub>2</sub> emissions from cities, *Geophys Res Lett*, 39, Artn L20802, doi  
6 10.1029/2012gl053087, 2012.
- 7 Pal, S., Xueref-Remy, I., Ammoura, L., Chazette, P., Gibert, F., Royer, P., Dieudonne, E.,  
8 Dupont, J. C., Haeffelin, M., Lac, C., Lopez, M., Morille, Y., and Ravetta, F.: Spatio-temporal  
9 variability of the atmospheric boundary layer depth over the Paris agglomeration: An  
10 assessment of the impact of the urban heat island intensity, *Atmos Environ*, 63, 261-275, Doi  
11 10.1016/J.Atmosenv.2012.09.046, 2012.
- 12 Pataki, D. E., Alig, R. J., Fung, A. S., Golubiewski, N. E., Kennedy, C. A., McPherson, E. G.,  
13 Nowak, D. J., Pouyat, R. V., and Lankao, P. R.: Urban ecosystems and the North American  
14 carbon cycle, *Global Change Biol*, 12, 2092-2102, Doi 10.1111/J.1365-2486.2006.01242.X,  
15 2006.
- 16 Pataki, D. E., Xu, T., Luo, Y. Q., and Ehleringer, J. R.: Inferring biogenic and anthropogenic  
17 carbon dioxide sources across an urban to rural gradient, *Oecologia*, 152, 307-322, Doi  
18 10.1007/S00442-006-0656-0, 2007.
- 19 Peylin, P., Rayner, P. J., Bousquet, P., Carouge, C., Hourdin, F., Heinrich, P., Ciais, P., and  
20 Contributors, A.: Daily CO<sub>2</sub> flux estimates over Europe from continuous atmospheric  
21 measurements: 1, inverse methodology, *Atmos Chem Phys*, 5, 3173-3186, 2005.
- 22 Prairie, Y. T., and Duarte, C. M.: Direct and indirect metabolic CO<sub>2</sub> release by humanity,  
23 *Biogeosciences*, 4, 215-217, 2007.
- 24 Shepson, P. B., Cambaliza, M., Davis, K., Gurney, K., Lauvaux, T., Richardson, N.,  
25 Richardson, S., Sweeney, C., and Turnbull, J.: Indianapolis flux experiment (INFLUX):  
26 Experiment design and new results regarding measurements of urban-area CO<sub>2</sub> and CH<sub>4</sub>  
27 emission fluxes, *Abstr Pap Am Chem S*, 242, 2011.
- 28 Tarantola, A.: Inverse problem theory and methods for model parameter estimation, Society  
29 for Industrial and Applied Mathematics, Philadelphia, PA, xii, 342 p. pp., 2005.
- 30 Widory, D., and Javoy, M.: The carbon isotope composition of atmospheric CO<sub>2</sub> in Paris,  
31 *Earth Planet Sc Lett*, 215, 289-298, Doi 10.1016/S0012-821x(03)00397-2, 2003.
- 32 Zhao, C. L., and Tans, P. P.: Estimating uncertainty of the WMO mole fraction scale for  
33 carbon dioxide in air, *J Geophys Res-Atmos*, 111, Artn D08s09, doi 10.1029/2005jd006003,  
34 2006.
- 35

## 1 Tables and captions

2

3 Table 1 : Information about the CO<sub>2</sub> measuring stations that are used in this paper.

4

Location	Acronym	Latitude [°]	Longitude [°]	Height AGL [m]	Distance from Paris centre [km]
Eiffel Tower	EIF	48.8582	2.2946	300	4 (W)
Montgé-en-Goële	MON	49.0284	2.7489	9	35 (NE)
Gonesse	GON	48.9908	2.4446	4	16 (N)
Gif sur Yvette	GIF	48.7100	2.1475	7	23 (SW)
Trainou Forest	TRN	47.9647	2.1125	180	101 (S)

5

6

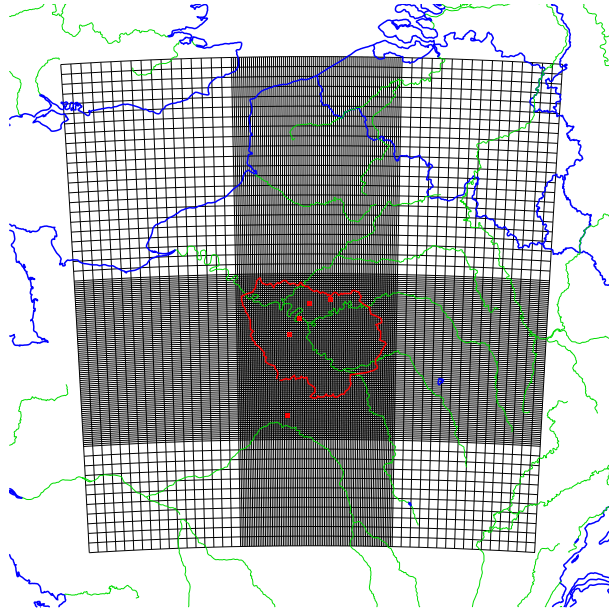


Figure 1 : Map of the study area showing the location of the continuous CO<sub>2</sub> measurement stations that are used in this paper (red dots). The black lines show the model grid with a 2 km resolution at the centre, and 10 km on the sides. The red line shows the limits of the Île-de-France region.

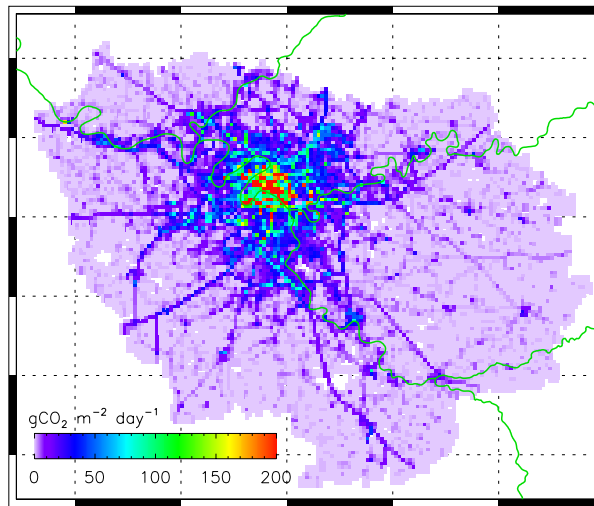


Figure 2 : Typical day-total CO<sub>2</sub> emissions of Île-de-France, according to AirParif year 2008 inventory, for a weekday in October. The point sources are not included in this map. The emissions are provided for the area outlined in red in Figure 1. The resolution is 1 km. The grid is 0.2° in latitude and 0.4° in longitude.

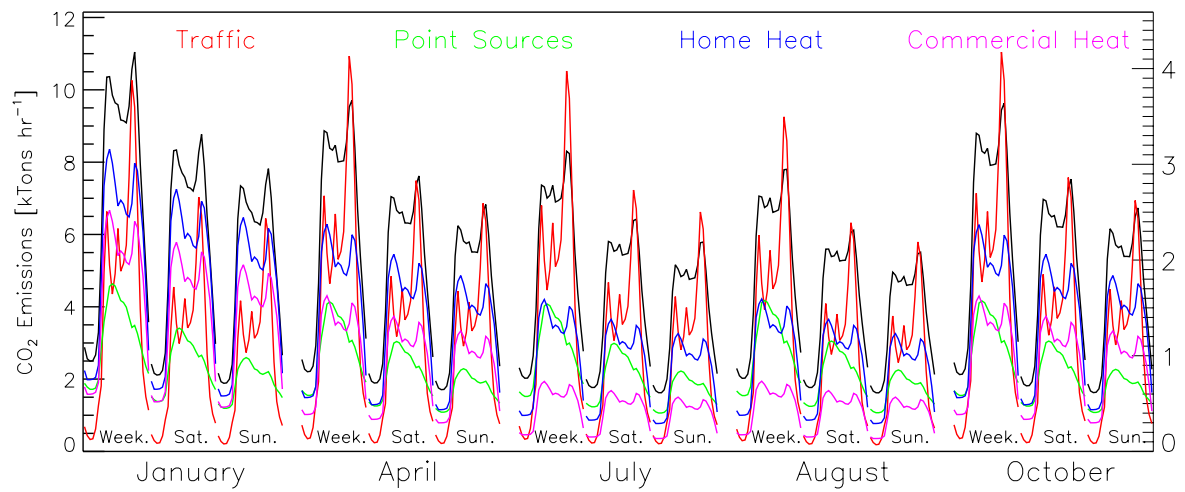


Figure 3: Temporal variation of the main CO<sub>2</sub> emission sectors according to the AirParif inventory for the whole Ile de France region. The figure shows, for 5 typical months and 3 typical days (Weekday, Saturday, Sunday), the hourly CO<sub>2</sub> emissions. The black line is the total emission (left scale) while the four coloured lines are for different sectors (right scale).

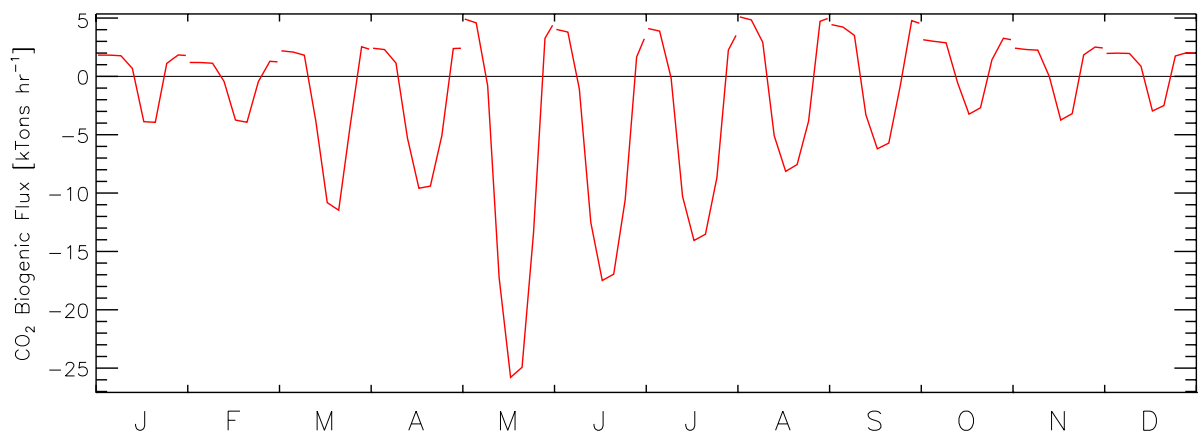


Figure 4: Mean diurnal cycle of the biogenic flux (Net Ecosystem exchange) for the 12 calendar months and for the same area as in Figures 2 and 3 which is outlined in red in Figure 1. The values were derived from an average of the C-Tessel simulations.



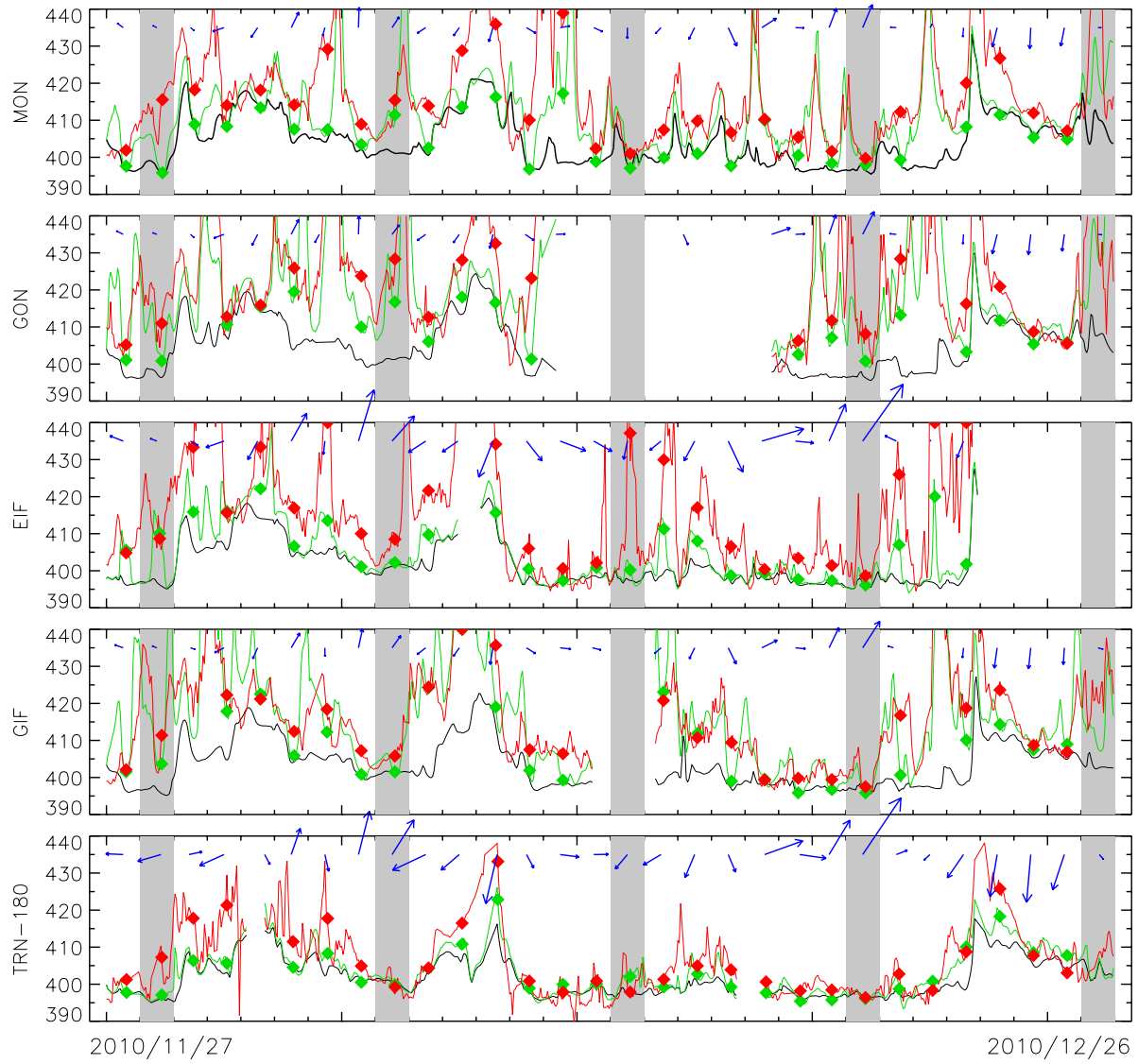


Figure 5: Time series of the measured (red) and modelled (green) CO<sub>2</sub> mole fraction [ppm] for the five sites used in this paper (See Table 1). The black line is the modelled mole fraction that is transported from the domain boundaries, with additional contribution from anthropogenic emissions outside the Île-de-France region (Edgar fluxes). The green line shows the modelled mole fraction that includes the same contributions, plus the biogenic fluxes within the modelling domain and the anthropogenic emissions within the Île-de-France region. Red are the observations. Note that there are some time periods when no measurements are available due to either calibration processes or, more rarely, failure of the monitoring instrumentation. For such periods, modelling results are not shown. The symbols show the mean of the afternoon measurement/model values that are used for the inversion. The blue arrows indicate the wind speed and direction at noon. A length equivalent to 1 day on the X-axis is for a wind speed of 10 m/s. Grey shaded areas indicate Sundays. This figure

is for the 30 days period starting on 2010/11/27. Figure S1 in the supplementary shows the same figure for the other period.

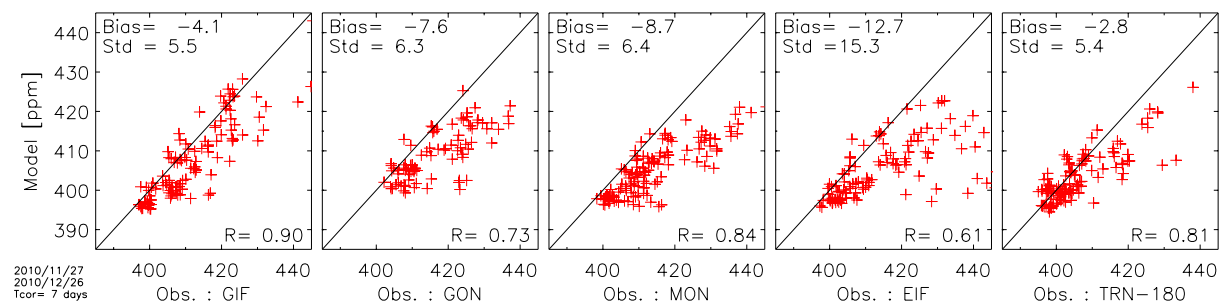


Figure 6 : Scatter plot of the measured and modelled CO<sub>2</sub> mole fractions at the 5 monitoring stations within and in the vicinity of the Paris city. The model vs measurement bias, standard deviation and correlations are provided within each subplot. This figure is for the 30 days period starting on 2010/11/27. Figure S2 in the supplementary shows the same figure for the other period.

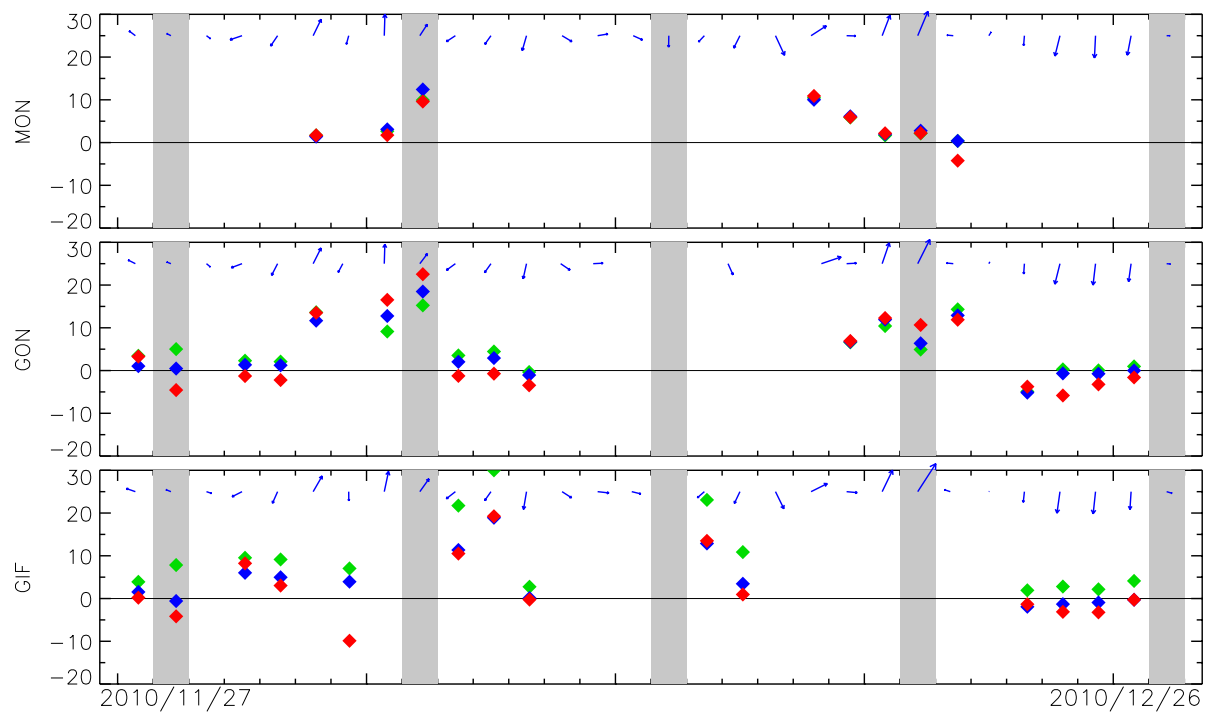


Figure 7 : Time series of the mole fraction differences between a station (Y-axis label) and another one used as a reference (either GIF or GON) and selected based on the wind direction (see section 3.3). The symbols show the mean afternoon concentrations (12AM-4PM) for the measurements (red), the prior (green) and the posterior (blue) estimates. As in Figure 5, the arrows indicate the wind speed and direction. A similar figure for the other time period is shown in the supplementary material.

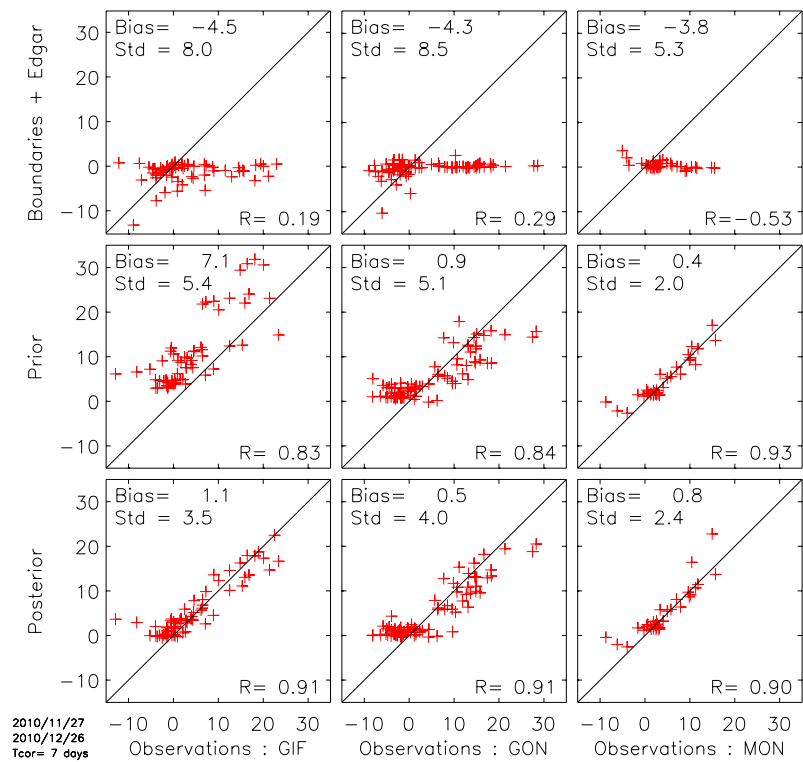


Figure 8 : Scatter plot of the measured and modelled concentration gradients for 3 downwind stations; either GIF or MON are used as an upwind reference. The first row shows the mole fraction simulated using the boundary conditions and the anthropogenic emissions outside Île-de-France ( $y_F$  in equation 1) against the measurements. The second row shows the concentration estimates derived from the prior values for the biogenic fluxes and anthropogenic fluxes against the corrected measurements (i.e.  $y - y_F$  in equation 1). The last row is the same but using the posterior estimates. This figure is for the Nov-Dec period. A similar figure for the other time period is shown in the supplementary material.

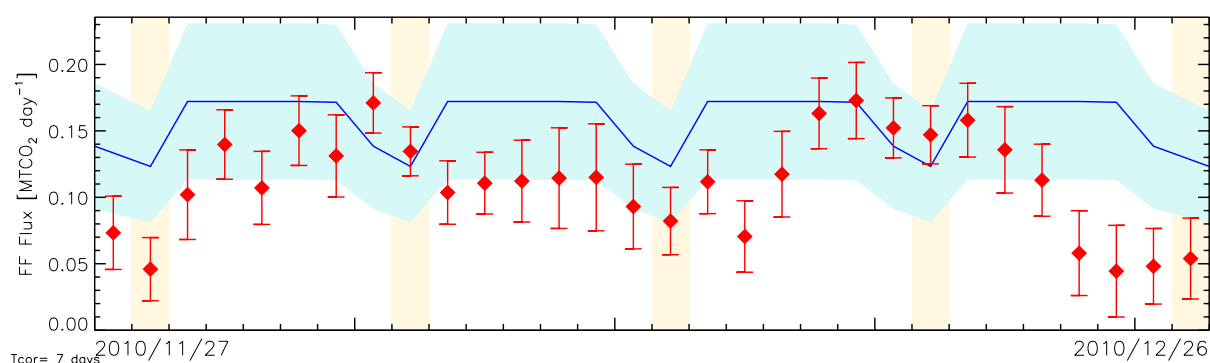
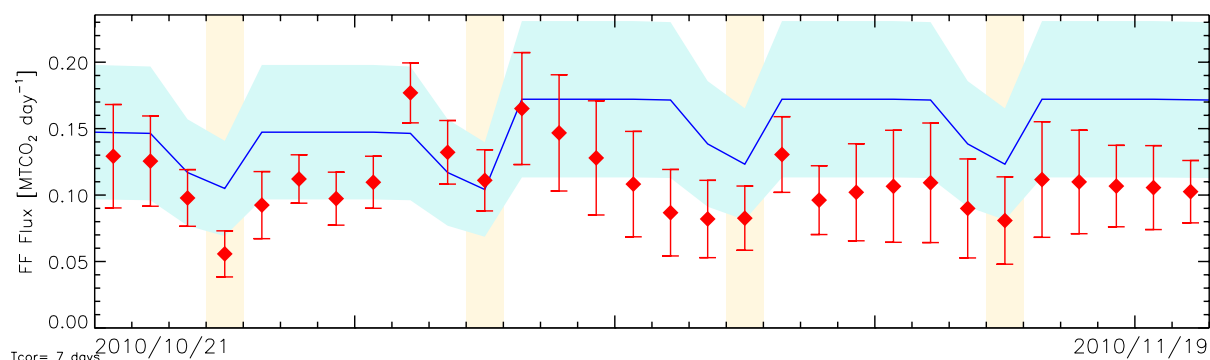
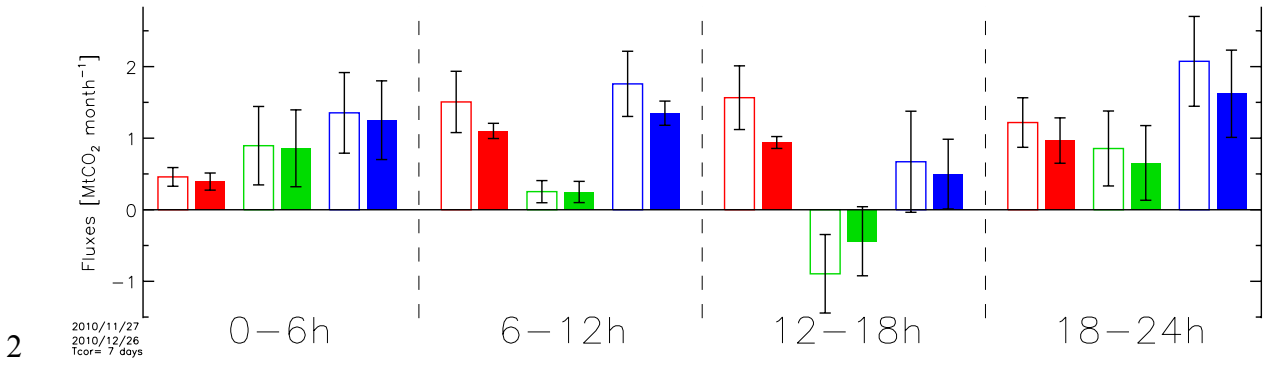
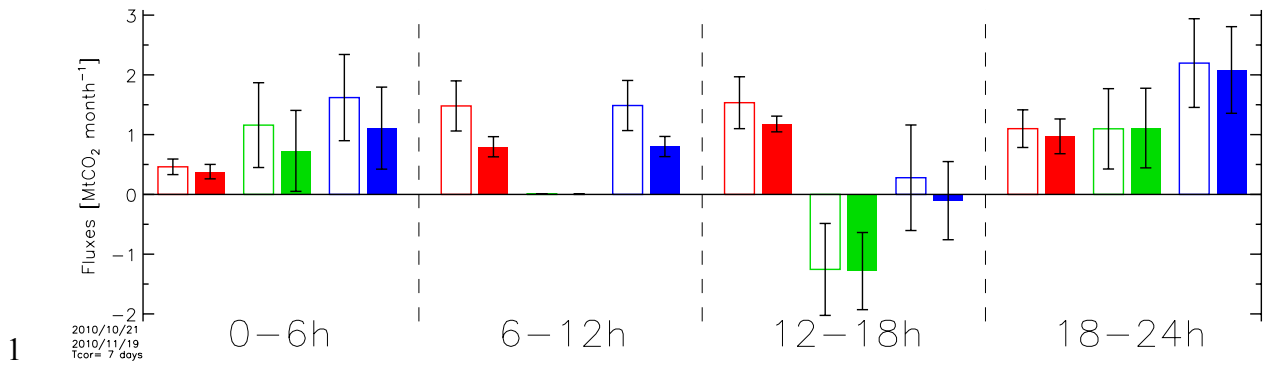


Figure 9 : Daily flux estimates of the anthropogenic emission for the 30 days of the period. The blue line and shading shows the prior flux according to the AirParif inventory together with its assumed uncertainty. Yellow shading indicate Sundays; note the weekly cycle with lower values during Saturdays and Sundays. The red symbols and bars show the posterior estimates with their uncertainty range. Both 30-day periods are shown.



3

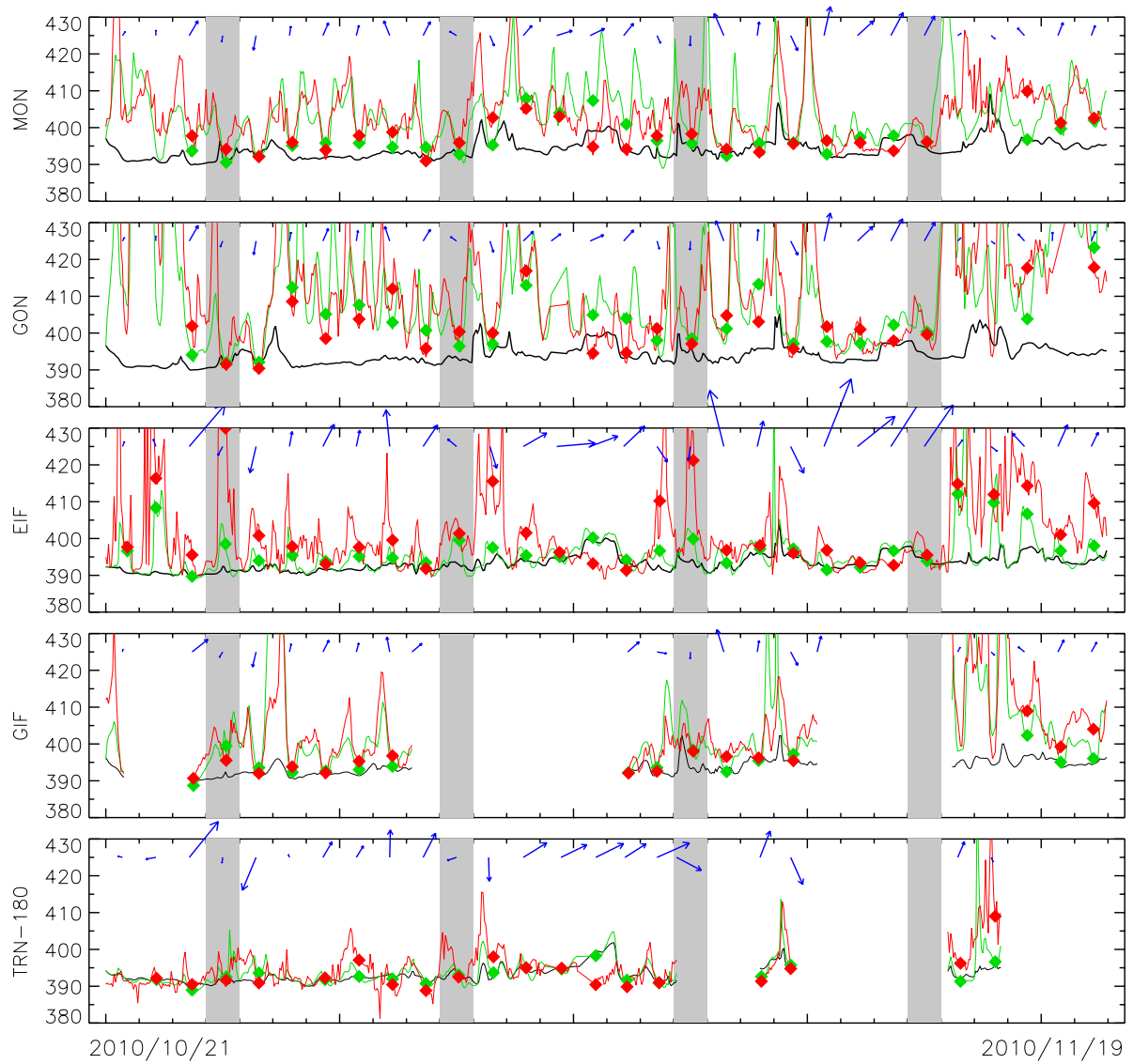
4 Figure 10 : Total flux estimates over the full 30 day period, for the 4 6-hour periods. Red is  
 5 for the anthropogenic emissions, green is for the biogenic fluxes while blue is for the total.  
 6 The prior estimates are shown as open rectangles while the posterior are shown as filled  
 7 rectangles. Both 30-day periods are shown independently.

8

9

# 1 Supplementary material

2



3

4 Figure S- 1: Same as Figure 5 but for the 30 days period starting on October 21<sup>st</sup>.

5

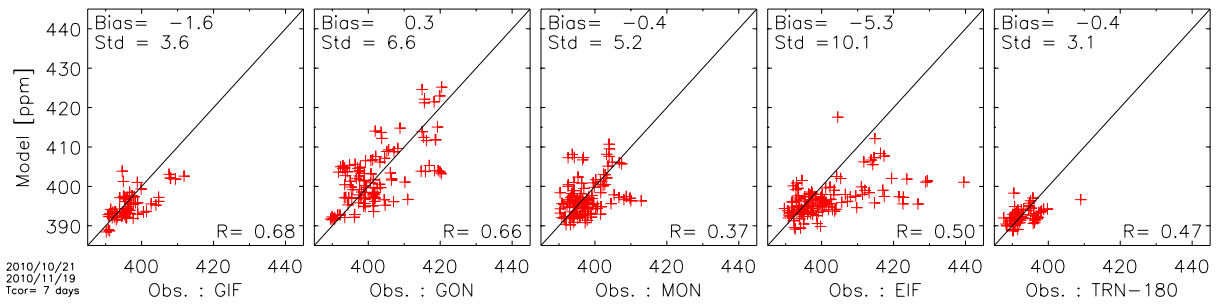


Figure S- 2 : Same as Figure 6 but for the 30 day period starting on October 21<sup>st</sup>.

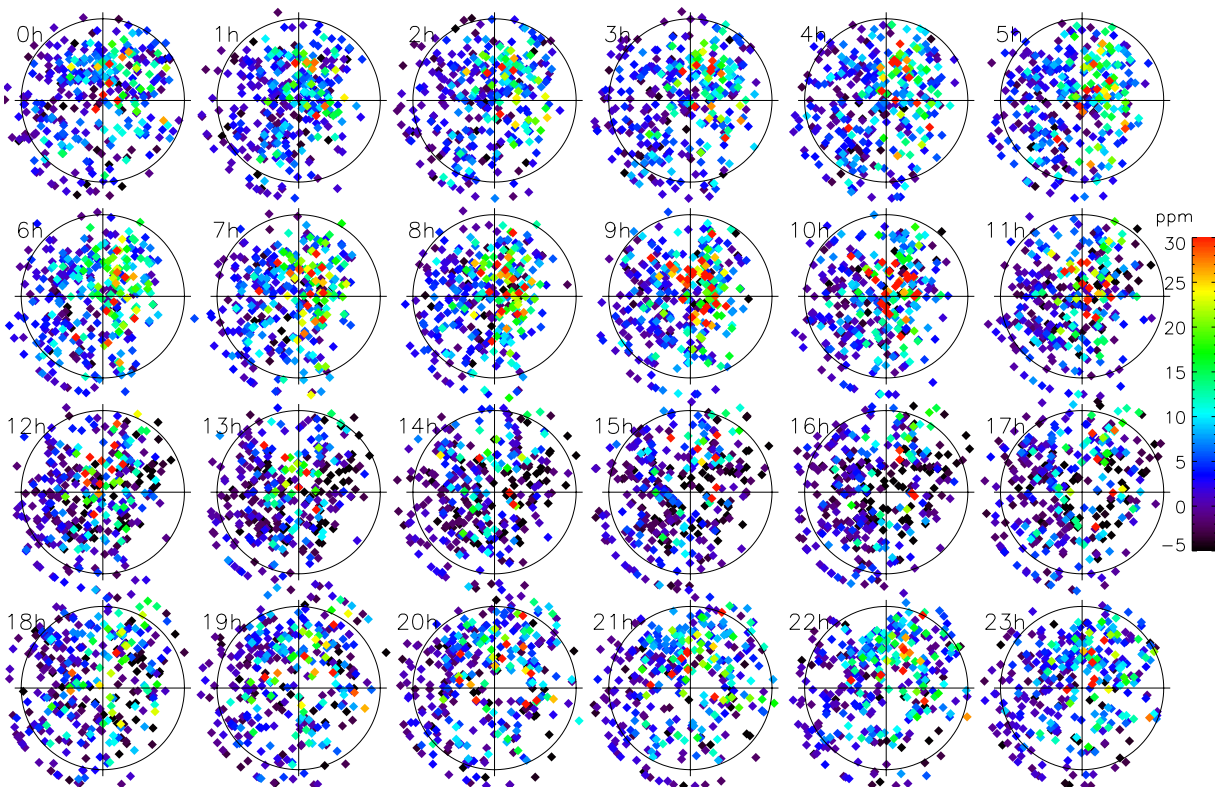


Figure S- 3 : Measurement-Model difference in CO<sub>2</sub> mole fraction at the EIF site as a function of time, wind speed and direction. The position of the symbols indicates the wind direction (top-right is for a wind from the North-East) and speed (the circles indicate a wind of 10 m s<sup>-1</sup>). The wind speeds have been bounded at 12 m s<sup>-1</sup>.



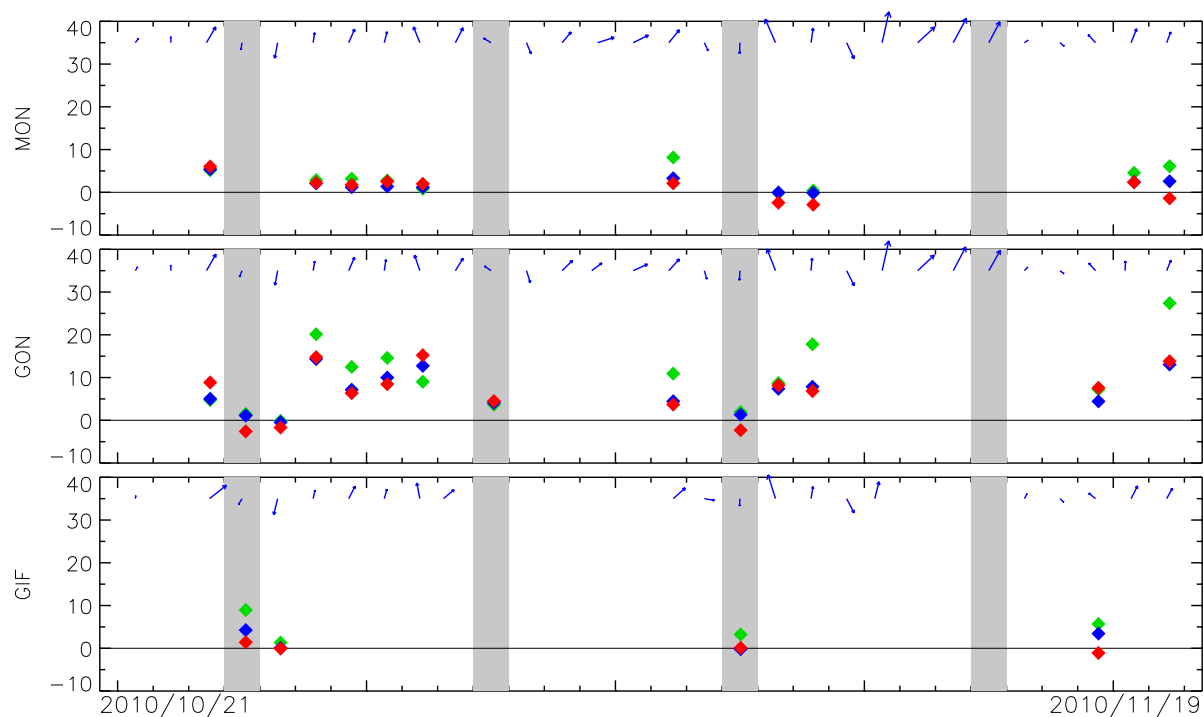


Figure S-4 : Same as Figure 7 but for the 30-day period starting on October 21<sup>st</sup>.

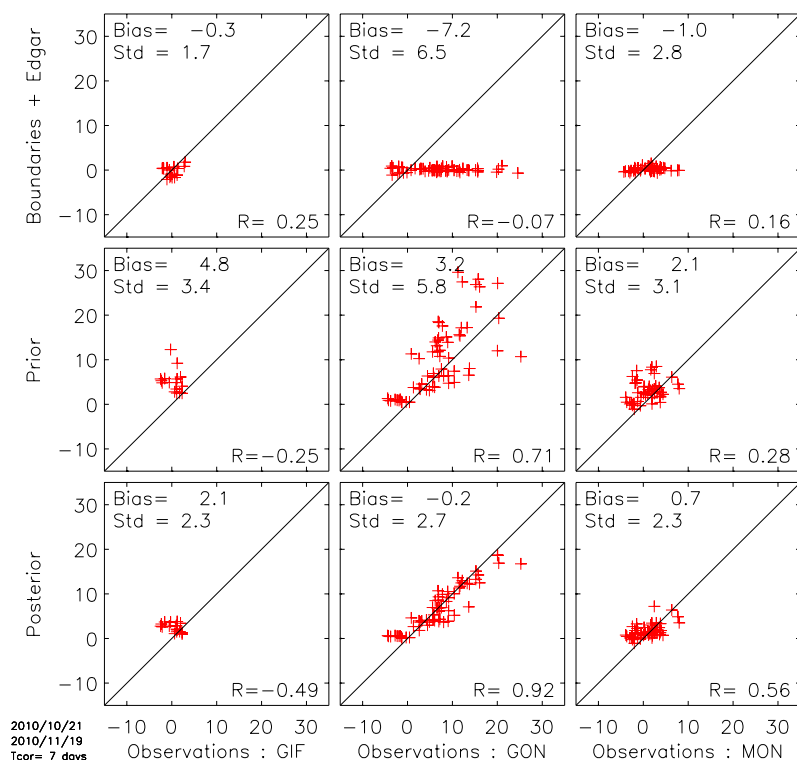


Figure S-5 : Same as Figure 8 but for the 30-day period starting on October 21<sup>st</sup>.